Evaluation of Trypanocidal Properties of Ferrocenyl and Cyrhetrenyl *N*-Acylhydrazones with Pendant 5-Nitrofuryl Group

Patricia M. Toro[a,*], Francisco Peralta[b], Juan Oyarzo[b], Shane R. Wilkinson[c], Mónica Zavala[c], Rodrigo Arancibia[d], Mauricio Moncada-Basualto[e], Iván Brito[f], Jonathan Cisterna[f], A. Hugo Klahn[b], Concepción López[g,*]

[a] Departamento de Ciencias Químicas, Facultad de Ciencias Exactas, Universidad Andrés Bello, Quillota 980, Viña del Mar, Chile.

[b] Instituto de Química, Pontificia Universidad Católica de Valparaíso, Casilla 4059, Valparaíso, Chile.

[c] School of Biological and Chemical Sciences, Queen Mary University of London, Mile End Road, London E1 4NS, UK.

[d] Facultad de Ciencias Químicas, Universidad de Concepción, Concepción, Chile.

[e] Departamento de Química Inorgánica y Analítica, Facultad de Ciencias Químicas y Farmacéuticas, Universidad de Chile, Santiago, Chile.

[f] Departamento de Química, Facultad de Ciencias Básicas, Universidad de Antofagasta, Avda. Universidad de Antofagasta 02800, Campus Coloso, Antofagasta, Chile.

[g] Departament de Química Inorgànica i Orgànica, Secció de Química Inorgànica, Facultat de Química, Universitat de Barcelona, Martí i Franqués 1-11, E-08028 Barcelona, Spain. E-mail: conchi.lopez@qi.ub.es

*Correspondence: p.torosanchez@uandresbello.edu (P. M. Toro), conchi.lopez@antares.qi.ub.edu (C. López).

Abstract

Four *N*-acylhydrazones of general formulae [R^1-C(O)-NH-N=C(R^2)(5-nitrofuryl)] with (R^1 = ferrocenyl or cyrhetrenyl and R^2 = H or Me) are synthesized and characterized in solution and in the solid-state. Comparative studies of their stability in solution under different experimental conditions and their electrochemical properties are reported. NMR studies reveal that the four compounds are stable in DMSO-d_6 and complementary UV-Vis studies confirm that they also exhibit high stability in mixtures DMSO:H_2O at 37 °C. Electrochemical studies show that the half-wave potential of the nitro group of the *N*-acylhydrazones is smaller than that of the standard drug nifurtimox and the reduction process follows a self-protonation mechanism. *In vitro* studies on the antiparasitic activities of the four complexes and the Nfx against *Trypanosoma cruzi* and *Trypanosoma brucei* reveal that: *i)* the *N*-acylhydrazones have a potent inhibitory growth activity against both parasites [EC_{50} in the low micromolar (in *T. cruzi*) or even in the nanomolar (in *T. brucei*) range] and *ii)* cyrhetrenyl derivatives are more effective than their ferrocenyl analogs. Parallel studies on the L_6 rat skeletal myoblast cell line have also been conducted, and the selectivity indexes determined. Three of the four *N*-acylhydrazones showed higher selectivity towards *T. brucei* than the standard drug nifurtimox. Additional studies suggest that the organometallic compounds are bioactivated by type I nitroreductase enzymes.

Keywords: Ferrocenyl *N*-acylhydrazones; cyrhetrenyl *N*-acylhydrazones; cyclic voltammetry; trypanocidal compounds; Type I nitroreductase.

1. Introduction

American trypanosomiasis (Chagas disease, CD) and Human African trypanosomiasis (HAT) are zoonotic, blood-borne, insect-transmitted infections caused by *Trypanosoma cruzi* (*T. cruzi*) and *Trypanosoma brucei* (*T. brucei*) parasites, respectively. Recent public health measures have substantially reduced the incidence and mortality of these diseases, but they still have a significant socio-economic impact on poor rural communities in Latin America and sub-Saharan Africa [1-6]. Treatments for CD and HAT are based on the use of drugs with potent trypanocidal activity [7-18], like nifurtimox (Nfx) [12], benznidazole [13] and megazol [14], (Fig. 1, A-C, respectively) for CD; pentamidine [15], melarsoprol (MelB) [16] (D and E in Fig. 1) or Nfx-eflornithine combination therapy for HAT [17]. Fexinidazole (Fig. 1, F), recently incorporated for HAT treatment, is now being tried against CD [18].

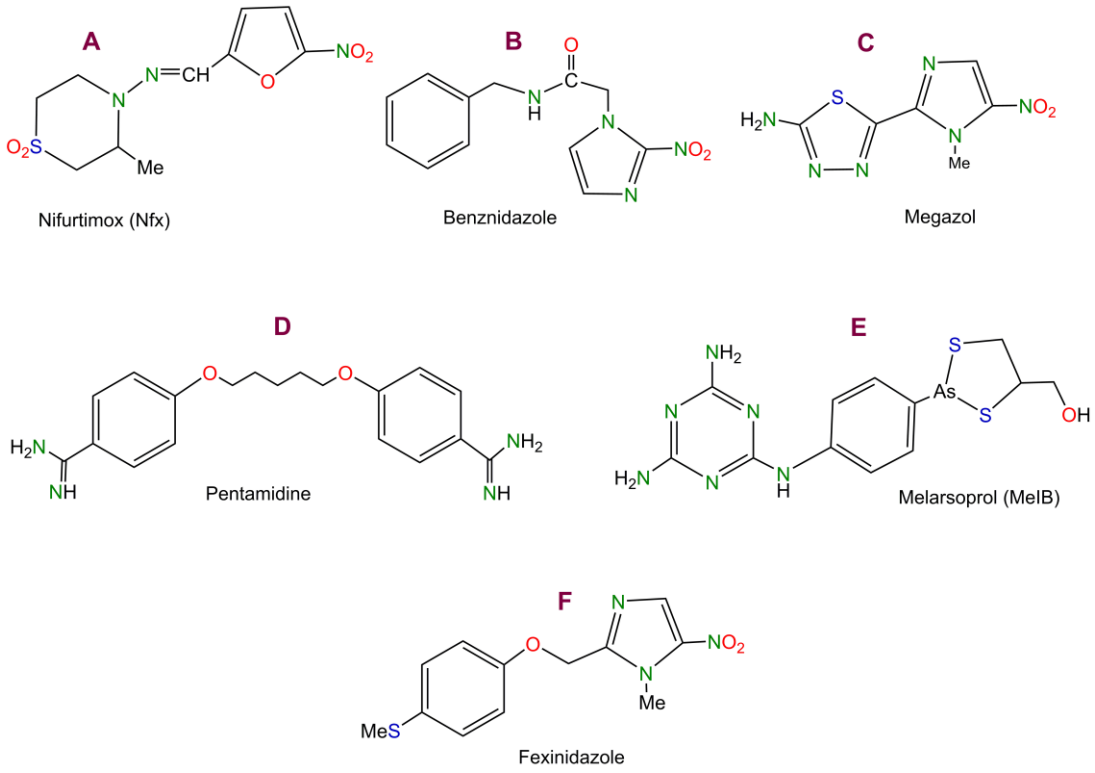

Figure 1. A selection of chemotherapeutic agents used for CD and HAT treatments [12 – 18].

Unfortunately, most of the chemotherapeutic agents shown in Fig. 1 cause severe and undesirable side effects and other problems arising from the lack of efficacy, sub-species specificity, drug resistance, cost, and administration [7-11,13,16,19,20]. Effective treatments for all the stages of CD and HAT are still unknown. The search for new drugs or prodrugs with improved activities and fewer side effects than those used nowadays is required and a top

priority in medicinal chemistry research [1-11]. Among the variety of strategies used to achieve more efficient chemotherapeutic agents, one better future expectations is based on new small molecules [21] combining bioactive cores or privileged scaffolds (i.e. thiosemicarbazone, hydrazine, *N*-acylhydrazone, heterocycles), relevant functional groups (as the $-NO_2$) or transition metal ions [22-33]. This strategy improves the absorption, distribution, metabolism, elimination, toxicity (ADMET properties [34]) of the drug and/or enhances its capability to block, inhibit or, in general, modify the action of key species (i.e. enzymes, proteins) that participate in the disease's progress.

Although the mechanism of action of most of the drugs presented in Fig. 1 has not been described in detail; it is widely accepted that the Nfx and other potent anti-CD or anti-HAT agents with a $-NO_2$ group are bioactivated by nitroreductases (NTRs) producing free radicals and/or cytotoxic metabolites that cause the cellular damage [35-37]. For these systems, the substituent's nature and location affect the proclivity of the $-NO_2$ group to be reduced and other properties relevant in biological media (i.e. lipophilicity and acidity) [38-40]. The selection and incorporation of the "adequate" substituents [privileged scaffolds, transition metal ions (M^{m+} and/or "$M(ligand)_n$" units or both simultaneously] on these heterocycles is one of the most promising paths to get new and more effective drugs for CD and HAT.

N-acylhydrazones (NAHs) are important scaffolds in drug design [22]. Potent anticancer, antiviral, antifungal, antiparasitic agents [41-47], and inhibitors of the action of biomolecules are known. The incorporation of the NAH unit in the backbones of drugs or biologically relevant scaffolds (i.e. heterocycles) and/or functionalities (i.e. the $-NO_2$) may produce compounds with varied biological properties and even different mechanisms of action. Examples of NAHs are shown in Fig. 2, of which A-C are used to treat severe infections [48-50]; while D is a potent anti-*Trichomonas vaginalis* agent [51].

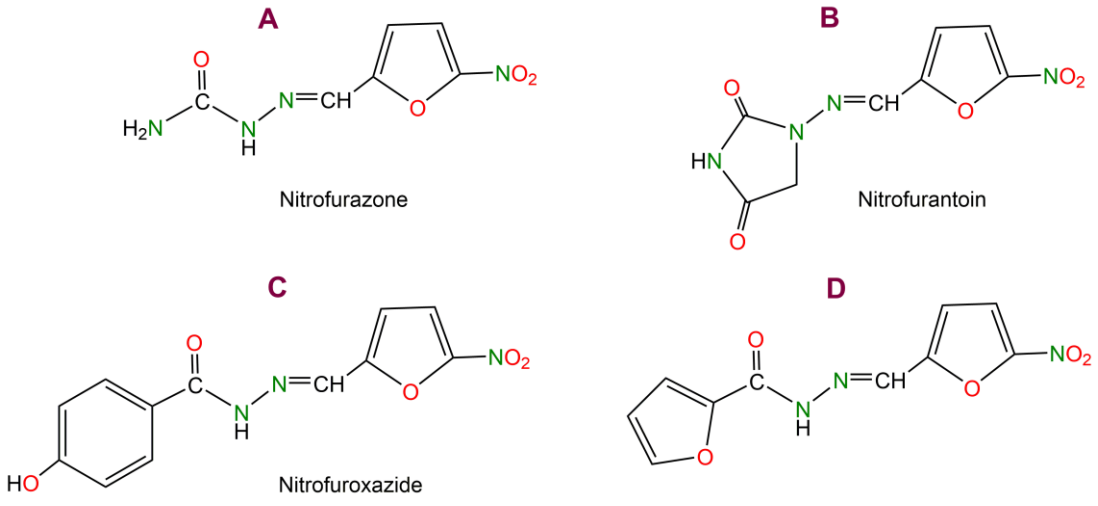

Figure 2. Small NAH molecules with the 5-nitrofuryl unit. Compounds A-C have been approved as topical antibacterial agents for treatments of genitourinary infections, diarrhea, and colitis (B and C) [48-50], and D reported recently is relevant for its outstanding anti-*trichomoniasis* potency [51].

It is well known that the binding of M^{m+} or "$M(ligands)_n$" units to bioactive molecules introduces significant changes in their conformation, structures, electronic distribution, and other properties important in drug design [29-33]. Complexes derived from mixed thiosemicarbazones-nitrofuryl ligands with relevant antiparasitic activities are known [52-54] and, those with NAH ligands are attractive due to their varied biological activities [55-57]. Among the wide variety of "$M(ligands)_n$" units available, organometallic arrays, especially those derived from ferrocene and cyrhetrene, are promising drug candidates to treat infective diseases, including trypanosomiasis [58-63].

For several years, we have reported ferrocenyl- and cyrhetrenyl- imines, amines, azines, benzoxazines, hydrazones, and sulfonamides, some of them with anticancer, antiparasitic, or antitubercular activities and low toxicity [62-71]. More recently, and mainly pushed by the necessity of new drugs for CD and HAT, we have focused our attention on small molecules (A-D in Fig. 3) combining the ferrocenyl/cyrhetrenyl array and the nitrofuryl (or thienyl) group [63-68]. Most of these products showed: *i)* anti-*T. cruzi* or anti-*T. brucei* activities similar to, or higher than, Nfx, and *ii)* even higher selectivity indexes. Thus, small molecules with the 5-nitrofuryl and ferrocenyl/cyrhetrenyl units are viewed as promising candidates to develop more potent and effective antiparasitic agents. NAHs with ferrocenyl units are scarce, and those with cyrhetrenyl groups are even less common [72]. Pyrazolyl, pyridinyl, aminobenzyl acylhydrazones with antibacterial, antitubercular, or antioxidant activities are known [73-76]. Carbonic anhydrase inhibitors based on ferrocenyl, cyrhetrenyl, and cymantrenyl acylhydrazones have been described recently [77].

Despite the ongoing interest in novel small molecules with *i)* 5-nitrofuryl units, *ii) N*-acylhydrazone arrays, and *iii)* metallocene derived moieties for new drug's design; their potential synergic effect has not been investigated so far and could lead to new and more effective anti-CD and anti-HAT agents.

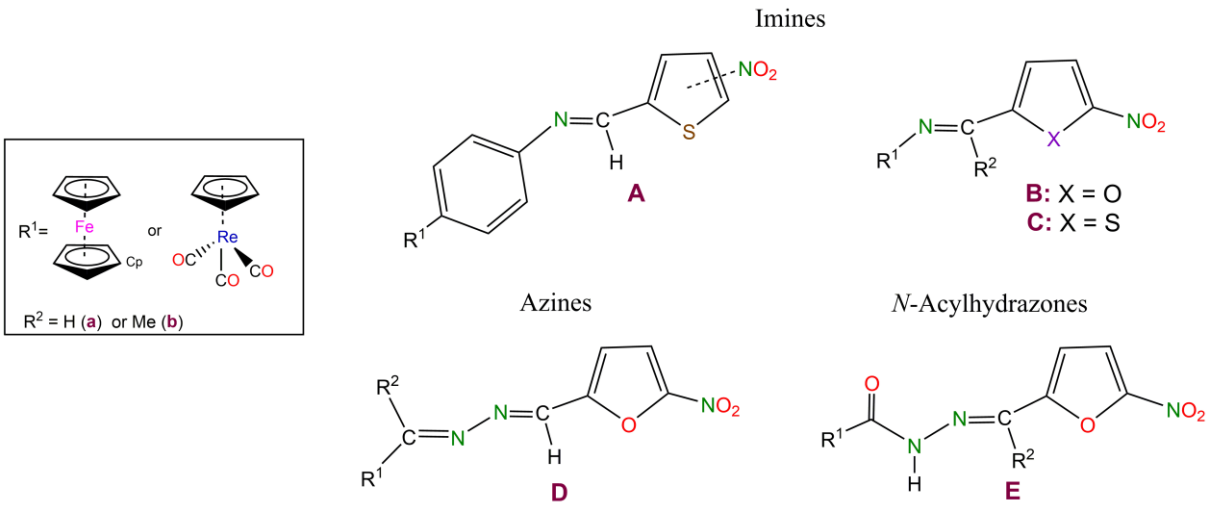

Figure 3. A selection of ferrocenyl and cyrhetrenyl imines (A-C) and azines (D) with potent antiparasitic activities reported recently [63-68], and the *N*-acylhydrazones (E) presented in this work.

In view of this, we focused our attention on ferrocenyl and cyrhetrenyl *N*-acylhydrazones E (Fig. 3), which can be visualized as derived from imines B by insertion of the -C(O)-NH- unit into the R^1-N bond. Here, we present a general procedure for preparing four type E compounds and a comparative study of their stability, electrochemical properties, biological activities against *T. cruzi* and *T. brucei*, their inhibitory growth effect on mammalian cells, and their bioactivation by type I NTR.

2. Experimental

2.1. Reagents and methods

All preparations were carried out using Schlenk techniques. The solvents were dried and distilled before use according to standard procedures [78]. 2-Acetylfuran (99%), 2-formyl-5-nitrofuran (99%) (**3a**), and trifluoroacetic acid (CF_3COOH, 99%) were obtained from Sigma Aldrich. The hydrazides [Fe(η^5-C_5H_5){(η^5-C_5H_4)-C(O)-NH-NH_2}] (**1**) and [Re{(η^5-C_5H_4)-C(O)-NH-NH_2}$(CO)_3$] (**2**) were prepared as reported previously [75,79], and a detailed description of the synthetic procedure used for 2-acetyl-5-nitrofuran (**3b**) [67] is included in the Electronic Supporting Information (ESI). Despite the synthesis of compounds **4a** and **4b** were briefly reported long ago, the procedure described in *section 2.2.*, based on the use of catalytic amounts of CF_3COOH, allows us to achieve the four *N*-acylhydrazones as crystalline materials and **4a** in shorter reaction periods (8 h versus 24 h) [72]. Infrared spectra (KBr disc) were recorded with a Jasco FT-IR 4600 spectrophotometer in the range of 4000 – 500 cm^{-1}. ^1H NMR spectra were recorded at room temperature on a Bruker Advance 300 spectrometer using

DMSO-d_6 (99.9%) as the solvent. Chemical shifts (δ), referenced to the deuterated residual solvent peaks, presented in ppm and the coupling constants (*J*) reported in Hertz (Hz). The electron impact mass spectra (EI-MS) were obtained on a Shimadzu QP5050A GC-MS mass spectrometer at the *Laboratorio de Servicios Analíticos, Pontificia Universidad Católica de Valparaíso*. Elemental analyses were obtained from Flash 2000 (Thermo Scientific) at the *Laboratorio Instrumental DCQ-Viña of Universidad Andrés Bello.* The stability studies were performed using a Agilent Cary 8454 Diode-Array Spectrophotometer in the range 250 – 650 nm. Each sample was prepared in concentration of 1×10^{-4} M in DMSO:H_2O (100:3). UV-Vis spectra were recorded at different times (*t*), keeping the sample at 37 °C by TC1 Temperature Controller for Quantum Northwest Peltier-Controlled Cuvette Holders.

*2.2. Synthesis of ferrocenyl and cyrhetrenyl N-acylhydrazones (**4a**,**b** and **5a**,**b**). General procedure*

A few drops of CF_3COOH were added to a mixture formed by 1.0 mmol amount of [Fe(η^5-C_5H_5){(η^5-C_5H_4)-C(O)-NH-NH_2}] (**1**) (244 mg) or [Re{(η^5-C_5H_4)-C(O)-NH-NH_2}$(CO)_3$] (**2**) (309 mg), and the equimolar amount of the appropriate 5-nitrofuran [**3a** (141 mg) or **3b** (155 mg)], and 15 mL of anhydrous ethanol (Scheme 1). The reaction mixture was then stirred under N_2 atmosphere at 80 °C for 5 h. After this period, the solid formed was separated by filtration, washed with ethanol, and dried in vacuum. These products were later purified at room temperature by crystallization in THF/hexane (1:5) mixtures.

Characterization data for [Fe(η^5-C_5H_5){(η^5-C_5H_4)-C(O)-NH-N=CH-(2-C_4H_2O-5-NO_2)}] (**4a**): Purple microcrystals. Yield: 77% (283 mg; 0.77 mmol). FT-IR (KBr, cm^{-1}): 3394 ν(NH); 1648 ν(CO); not observed ν(C=N). ^{1}H NMR (DMSO-d_6): δ 4.23 (s, 5H, Cp); 4.51 (s, 2H, H^3 and H^4); 4.97 (s, 2H, H^2 and H^5); 7.24 (s, 1H, H^6); 7.81 (s, 1H, H^7); 8.40 (s, 1H, CH=N); 11.6 (s, 1H, NH). EI-MS (*m/z*): 367 $[M]^+$; 302 $[M - Cp]^+$; 213 $[M - (NH\text{-}N{=}CH\text{-}C_4H_2O)\text{-}(NO_2)]^+$; 185 $[M - (CO\text{-}NH\text{-}N{=}CH\text{-}C_4H_2O)\text{-}(NO_2)]^+$. Anal. (%) Calc. for $C_{16}H_{13}N_3O_4Fe$: C, 52.34; H, 3.57 and N, 11.45; found: C, 52.59; H, 3.58 and N, 11.42. UV-Vis (for = 0 h) λ_{max} = 385 nm; extinction coefficient ε = 4.2 M^{-1} cm^{-1}.

Characterization data for [Fe(η^5-C_5H_5){(η^5-C_5H_4)-C(O)-NH-N=C(Me)-(2-C_4H_2O-5-NO_2)}] (**4b**): Dark red crystals. Yield: 67% (255 mg; 0.67 mmol). FT-IR (KBr, cm^{-1}): 3421 ν(NH); 1634 ν(CO); 1594 ν(C=N). ^{1}H NMR (DMSO-d_6): δ 2.31 (s, 3H, Me); 4.22 (s, 5H, Cp); 4.50 (s, 2H, H^3 and H^4); 5.08 (s, 2H, H^2 and H^5); 7.26 (s, 1H, H^6); 7.80 (s, 1H, H^7); 10.5 (s, 1H, NH).

EI-MS (*m/z*): 381 $[M]^+$; 316 $[M - Cp]^+$; 213 $[M - (NH\text{-}N{=}C(Me)\text{-}C_4H_2O)\text{-}(NO_2)]^+$; 185 $[M - (CO\text{-}NH\text{-}N{=}C(Me)\text{-}C_4H_2O)\text{-}(NO_2)]^+$. Anal. (%) Calc. for $C_{17}H_{15}N_3O_4Fe$: C, 53.57; H, 3.97 and N, 11.02; found: C, 53.38; H, 3.95 and N, 11.02. UV-Vis (for = 0 h) λ_{max} = 385 nm; extinction coefficient ε = 4.1 M^{-1} cm^{-1}.

Characterization data for $[Re\{(\eta^5\text{-}C_5H_4)\text{-}C(O)\text{-}NH\text{-}N{=}CH\text{-}(2\text{-}C_4H_2O\text{-}5\text{-}NO_2)\}(CO)_3]$ (**5a**): Light brown solid. Yield: 63% (325 mg; 0.63 mmol). FT-IR (KBr, cm^{-1}): 3430 ν(NH); 2026 $\nu(CO)_{Re}$; 1926 $\nu(CO)_{Re}$; 1654 ν(CO); not observed ν(C=N). ^{1}H NMR (DMSO-d_6): δ 5.82 (t, 2H, H^3 and H^4); 6.45 (s, 2H, H^2 and H^5); 7.29 (d, 1H, *J* = 4.0, H^6); 7.81 (d, 1H, *J* = 4.0, H^7); 8.32 (s, 1H, CH=N); 11.9 (s, 1H, NH). EI-MS (*m/z*) (based on ^{187}Re): 517 $[M]^+$; 489 $[M - CO]^+$; 433 $[M - 3CO]^+$; 363 $[M - (NH\text{-}N{=}CH\text{-}C_4H_2O)\text{-}(NO_2)]^+$; 335 $[M - (CO\text{-}NH\text{-}N{=}CH\text{-}C_4H_2O)\text{-}(NO_2)]^+$. Anal. (%) Calc. for $C_{14}H_8N_3O_7Re$: C, 32.56; H, 1.56; and N, 8.14; found: C, 32.47; H, 1.55; and N, 8.17. UV-Vis (for = 0 h) λ_{max} = 380 nm; extinction coefficient ε = 4.1 M^{-1} cm^{-1}.

Characterization data for $[Re\{(\eta^5\text{-}C_5H_4)\text{-}C(O)\text{-}NH\text{-}N{=}C(Me)\text{-}(2\text{-}C_4H_2O\text{-}5\text{-}NO_2)\}(CO)_3]$ (**5b**): Yellow crystals. Yield: 53% (281 mg; 0.53 mmol). FT-IR (KBr, cm^{-1}): 3433 ν(NH); 2027 $\nu(CO)_{Re}$; 1652 ν(CO); 1608 ν(C=N). ^{1}H NMR (DMSO-d_6): δ 2.26 (s, 3H, Me); 5.81 (s, 2H, *J* = 2.4, H^3 and H^4); 6.57 (s, 2H, H^2 and H^5); 7.28 (d, 1H, *J* = 4.0, H^6); 7.79 (d, 1H, *J* = 4.0, H^7); 11.3 (s, 1H, NH). EI-MS (*m/z*) (based on ^{187}Re): 531 $[M]^+$; 503 $[M - CO]^+$; 447 $[M - 3CO]^+$; 363 $[M - (NH\text{-}N{=}C(Me)\text{-}C_4H_2O)\text{-}(NO_2)]^+$; 335 $[M - (CO\text{-}NH\text{-}N{=}C(Me)\text{-}C_4H_2O)\text{-}(NO_2)]^+$. Anal. (%) Calc. for $C_{15}H_{10}N_3O_7Re$: C, 33.96; H, 1.90; and N, 7.92; found: C, 34.05; H, 1.90; and N, 7.95. UV-Vis (for = 0 h) λ_{max} = 380 nm; extinction coefficient ε = 4.1 M^{-1} cm^{-1}.

2.3. Crystal structure determination

Crystallographic data for **2** and **4b** were collected on a D8 Venture diffractometer equipped with a bidimensional CMOS Photon 100 detector, using graphite monochromated Mo-Kα (λ = 0.71073 Å) radiation. The diffraction frames were integrated using the APEX3 package [80] and were corrected for absorptions with SADABS [81]. The structures of **2** and **4b** were solved by intrinsic phasing [82] using the OLEX2 [83]. Both structures were then refined with full-matrix least-squares methods based on F^2 (*SHELXL-2014*) [82]. All non-hydrogen atoms were refined with anisotropic displacement parameters. All H-atoms were positioned geometrically with C-H = 0.93, N-H = 0.86, -NH_2 = 0.89 Å and refined using a riding model with $U_{iso}(H)$ = $1.2U_{eq}(C,N)$. A summary of crystal data, collection parameters, and refinement are presented

in Table S1; additional crystallographic details are included in the CIF files and ORTEP views were drawn using OLEX2 software [83].

2.4. Electrochemical Studies

Electrochemical characterization was performed under recommended experimental conditions with slight modification [84]. Cyclic voltammetry studies were carried out at room temperature using a 693 VA Metrohm instrument equipped with a 694 VA Stand converter and 693 VA processor in a three-electrode cell. A hanging drop of mercury (HMDE) working electrode, a platinum auxiliary electrode, and a non-aqueous Ag/AgCl reference electrode were used. Each complex was dissolved in DMSO containing 0.1 mol L^{-1} of tetrabutylammonium perchlorate (TBAP) as a supporting electrolyte to generate 1.0×10^{-3} mol L^{-1} final concentration. All electrolyte solutions were thoroughly pre-purged using purified nitrogen gas before use. Cyclic voltammograms (CVs) of the ferrocene under identical conditions were performed before and after each experiment to check the non-aqueous Ag/AgCl stability of the electrode. The measurements were performed at scan rates v = 0.10, 0.25, 0.50, 1.00, 1.50 and 2.00 V s^{-1}.

2.5. Biological Studies

2.5.1. Cell culturing

Trypanosoma cruzi Cl-Brener epimastigotes were grown at 25 °C in RPMI-1640 (Roswell Park Memorial Institute medium) medium supplemented with 4.9 mg mL^{-1} trypticase, 20 mM HEPES [4-(2-hydroxyethyl)piperazine-1-ethanesulfonic acid] pH 7.4, 2.0 mM sodium glutamate, 2.0 mM sodium pyruvate, 2.5 U mL^{-1} penicillin, 2.5 µg mL^{-1} streptomycin and 10% (v/v) heat-inactivated fetal calf serum [85,86].

Trypanosoma brucei [MITat 427 strain; clone 221a, and a derivative (2T1) that constitutively expresses the tetracycline repressor protein] bloodstream form (BSF) trypomastigotes were grown at 37 °C under a humid 5.0% (v/v) CO_2 atmosphere and in Hirumis' modified Iscoves' 9 medium as previously described [87,88]. 2T1 and a recombinant version that can be tetracycline (1 µg mL^{-1}) induced to overexpress *T. brucei* NTR1 (TbNTR1) were maintained in this medium, supplemented with 1 µg mL^{-1} phleomycin and/or 2.5 µg mL^{-1} hygromycin [20].

Rat skeletal myoblast cells (L_6) were grown at 37 °C under a 5.0% (v/v) CO_2 atmosphere in RPMI-1640 medium supplemented with 20 mM HEPES pH 7.4, 2.0 mM sodium glutamate, 2.0 mM sodium pyruvate, 2.5 U mL^{-1} penicillin, 2.5 mg mL^{-1} streptomycin and 10% (v/v) fetal calf serum (Pan Biotech UK Ltd).

2.5.2. Anti-proliferative assays

The following growth inhibition assays were carried out in a 96-well plate format. *T. cruzi* epimastigotes, *T. brucei* BSF trypomastigotes, or L_6 rat skeletal myoblasts were seeded at 5×10^5, 1×10^4 or 1×10^4 cells mL^{-1}, respectively, in 200 µL growth medium containing different compound concentrations. Compounds were prepared as 10 mM stock solutions in 100% (v/v) DMSO and stored at −20 °C before use. Then, serial dilutions were carried and the final concentration of DMSO in the culture medium never exceed 1%. After incubation, at 25 °C for 10 days (*T. cruzi*), or 37 °C for 3 (*T. brucei*), or 6 days (L_6 cells), resazurin (Sigma Aldrich) was added to each well to a final concentration of 12.5 mg mL^{-1} (or 2.5 mg per well). The plates were further incubated at 25 °C for 16 h (*T. cruzi*), or 37 °C for 8 h (*T. brucei* and L_6 cells) before measuring the fluorescence of each culture using a Gemini Fluorescent Plate reader (Molecular Devices) set at λ_{ex} = 530 nm, and λ_{em} = 585 nm with a filter cut off at 550 nm. The change in fluorescence resulting from the reduction of resazurin was proportional to the number of live cells. The compound concentration of each compound that inhibits cell growth by 50% (EC_{50}) was determined using the non-linear regression tool on GraphPad Prism (GraphPad Software Inc.), and the statistical significance of any differences in parasite susceptibilities was assessed using the Student's t-test calculator [89].

3. Results and discussion

3.1. Synthesis and characterization

The *N*-acylhydrazones were prepared by a condensation reaction and following the previously described procedure for [Re{(η^5-C_5H_4)-C(O)-NH-N=C(Me)-(2-C_4H_2S)}$(CO)_3$] [79], but using the hydrazides (**1** or **2**) and the corresponding 2-formyl- or 2-acetyl-5-nitrofuran (**3a** and **3b**, respectively). The reactions were performed in ethanol and in the presence of catalytic amounts of CF_3COOH (Scheme 1). The *N*-acylhydrazones are air-stable solids at room temperature and exhibit moderate solubility in THF and DMSO, but they are practically insoluble in hexane.

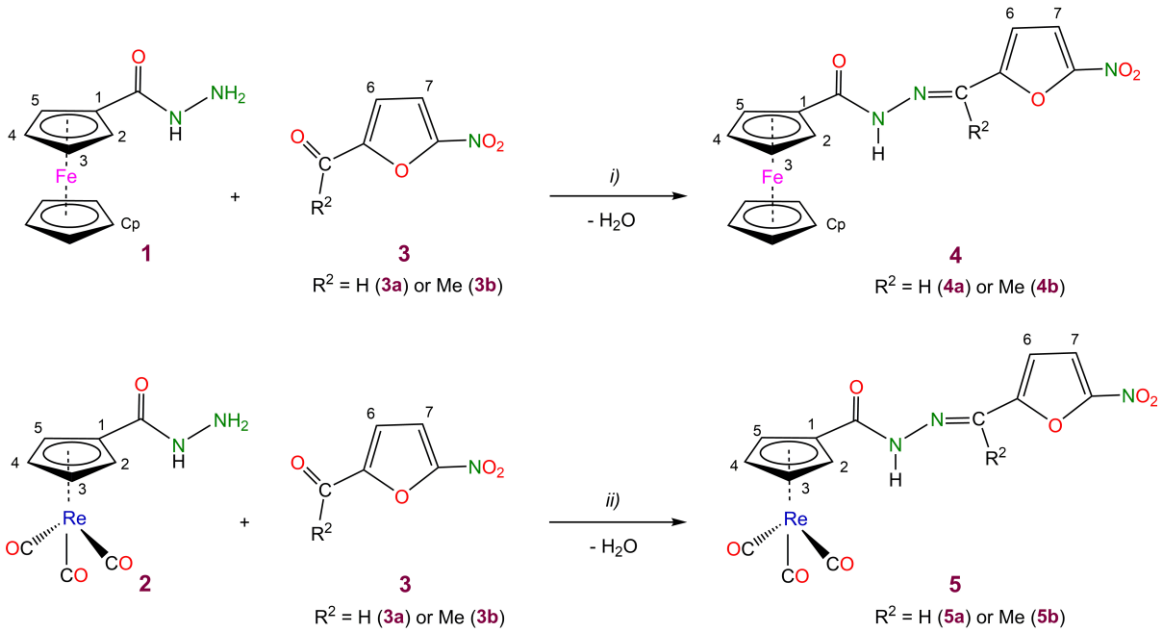

Scheme 1. Synthesis of the compounds. Reagents and conditions: for steps *i)* and *ii)*: equimolar amounts of the reagents, in absolute ethanol at 80 °C for 5 h, and in the presence of CF_3COOH catalytic amounts. Labels refer to the numbering pattern used for the assignment of NMR data.

Elemental analyses of compounds **4a**, **4b**, **5a**, and **5b** are consistent with the proposed formulae (see *section 2.2.*). Their mass spectra (Figs. S1 – S4) displayed molecular ion peak at *m/z* 367, 381, 517, and 531, respectively, in agreement with the calculated values for the corresponding molecular cations $[M]^+$. A common fractionation pattern, with loss of the fragments [-NH-N=C(R^2)-C_4H_2O-NO_2] and [-C(O)-NH-N=C(R^2)-C_4H_2O-NO_2] (R^2 = H, Me) was evident in all cases. In the MS spectra of the cyrhetrenyl compounds **5a** and **5b**, additional peaks arising from loss of the CO ligands attached to the Re(I) atoms were also detected.

The compounds were also characterized in solution by ^{1}H NMR. Since the solvent used for the electrochemical studies and preparing stock solutions of the compounds for the biological studies (see below) was DMSO, the ^{1}H NMR studies were carried out in DMSO-d_6. In all cases, the ^{1}H-NMR spectra (Figs. S5 – S8) exhibited a rather broad singlet in the low-field region (10.5 – 11.9 ppm) assigned to the -NH proton [74,90]. Based on this peak, the influence of the opposite electronic effects of the organometallic fragments could be established. In cyrhetrene derivatives (electron-withdrawing), this signal is low-field shifted relative to their ferrocenyl analogs (electron-donating). For **4a** and **5a** (Figs. S5 and S7), the singlets at δ = 8.40 and 8.32 are due to the imine proton, respectively, while for **4b** and **5b**, the resonance of the methyl protons appeared nearby 2.30 ppm. The position of these signals agrees with those reported for

azines D (shown in Fig. 3) [91]. All these findings confirm the existence of the -NH-N=C(R^2)- arrays (R^2 = H or Me) in the new products.

NMR studies provided conclusive evidence of the presence of only one isomer in the DMSO-d_6 solution at room temperature. The chemical shift of the imine proton agrees with those reported for related ferrocenyl and cyrhetrenyl Schiff bases that adopt the *E*-form in solution [70]. Besides, when models of the *Z*-form of the compounds were built using a molecular model kit, it became evident that the *cis*-disposition of the substituents on the -N=CH- unit introduces significant steric effects. For a coplanar arrangement between the furyl unit and the -N-N=C- array, the amine hydrogen is very close to either one of the heterocycle's hydrogen atoms or the oxygen atom. On these bases, we assume that the compounds also adopt the *E*-form in DMSO-d_6.

In all cases, two resonances observed in the range $7.4 < \delta < 7.8$ ppm were assigned to protons on the 5-nitrofuryl ring (H^6, H^7). Their chemical shifts are similar to those reported for imines and azines A-D (shown in Fig. 3) [65,91]. As expected, the spectra of **4a** and **4b** showed a set of three signals in the range 4.22 – 5.08 ppm of relative intensities 5:2:2 that correspond to the three types of protons [Cp and the pairs (H^2, H^5) and (H^3, H^4)] of the ferrocenyl unit; while for their Re(I) analogs (**5a** and **5b**), two signals were observed in the range 5.81 – 6.57 ppm attributed to the resonances of the cyrhetrenyl unit [62,77,92]. Due to the low definition of the signals detected in the spectra, some resonances of the protons of the C_5H_4 unit appeared as singlets. It should be noted that the magnitude of coupling constants is small [$^3J(H,H) < 2.3$ ppm] [65-67]. Unfortunately, the low solubility of all the compounds in deuterated solvents precluded us from measuring their ^{13}C NMR spectra to fulfill their characterization.

It is widely accepted that the stability of compounds (in the solid-state and solution) is important in view of their potential utility as candidates for new drugs. As mentioned in the preceding sections, the complexes **4** and **5** are highly stable in the solid-state. In order to check their stability in solution, we first compared the ^1H NMR spectra of freshly prepared solutions of the compounds in DMSO-d_6 with those registered after several periods of storage at 0 °C (Figures S9 and S10). For **4b** and **5b**, no significant changes in their NMR spectra were detected after several weeks of storage, indicating that these compounds are stable under these experimental conditions.

In view of the problems arising from the moderate solubility of the compounds in DMSO-d_6, the low definition of the ^1H NMR spectra, and in order to get further information of their stability in solution, additional studies based on UV-Vis spectroscopy were carried out. In all

cases, UV-Vis spectra of the complexes in DMSO:H_2O (100:3) mixtures were registered at the same temperature (37 °C) used during incubation of the samples with *T. cruzi* parasites and L_6 cells (see *section 2.5.2.*). The absorption spectrum of the initial solution (t = 0) was then compared with those obtained every 3 h after storage at 37 °C. All spectra (Figs. S11 – S14) show an intense band (log ε ≈ 4.1) in the range 380 ≤ λ_1 ≤ 385 nm. For compounds **4a** and **4b** the intensity of this band decreases gradually [log ε_1 = 4.1 (t = 0) and 4.0 (t = 24 h) Figs. S11 – S12]; while for compounds **5a** and **5b**, no significant change was observed in their UV-Vis spectra as the storage time increased from t = 0 to 24 h (Figs. S13 – S14). These results indicate that the Re(I) compounds (**5a** and **5b**) are more stable than their ferrocenyl analogs (**4a** and **4b)** under these experimental conditions.

The IR spectra of compounds **4a,b** and **5a,b** are shown in Figs. S15 – S18, and a summary of the most relevant bands detected are presented in *section 2.2*. The IR spectra of **4b** and **5b** (in solid-state) exhibited a narrow absorption due to the ν(C=N) bond at 1594 and 1608 cm^{-1}, respectively. This absorption was not observed in compounds **4a** and **5a**; apparently, the ν(C=N) band is overlapped with that of the *N*-acyl unit's CO group. This was also observed related compounds derived from 2-acetyl-5-nitrothiophene [79]. As expected, the additional absorption band detected at ca. 1654 – 1634 cm^{-1} (for **4a** and **4b**) and around 1653 cm^{-1} (for **5a** and **5b**) is assigned to the -C(O)- unit of the *N*-acylhydrazone. This band's position is similar to those reported for other ferrocenyl and cyrhetrenyl derivatives [79,90]. Another common feature of all spectra is a medium intensity band in the range 3433 – 3394 cm^{-1}, due to the -NH- unit's stretching. The two absorption bands detected in the IR spectra of compounds **5a** and **5b** in the range 2027 – 1926 cm^{-1} are due to the CO ligands bound to the Re(I) center.

*3.2. X-ray crystal structure of **4b***

As mentioned above, the synthesis and NMR spectra of cyrhetrenyl hydrazide (**2**) was recently reported by our group [79]. Despite the importance of intermolecular contacts in hydrazides and acylhydrazones, the crystalline structure of **2** remained unknown. In order to fill this gap, monocrystals of **2** were obtained. The crystal structures of compounds **2** and **4b** were determined by X-ray diffraction (Tables S2 – S5). A detailed description of the crystalline structure of compound **2** is included in the ESI.

In the molecular structure of compound **4b**, the relative arrangement of the substituents on the -CH=N- is *trans*, and therefore its configuration is *E* (Fig. 4). The ferrocenyl fragment

adopted an eclipsed conformation, similar to that found in [Fe(η^5-C_5H_5){(η^5-C_5H_4)-CH=N-NH-C(O)-(2-C_4H_3O)}] [90]. The distances Fe-centroid of the "C_5H_4" and "C_5H_5" rings fall in the range expected for related ferrocenyl *N*-acylhydrazones [74,90].

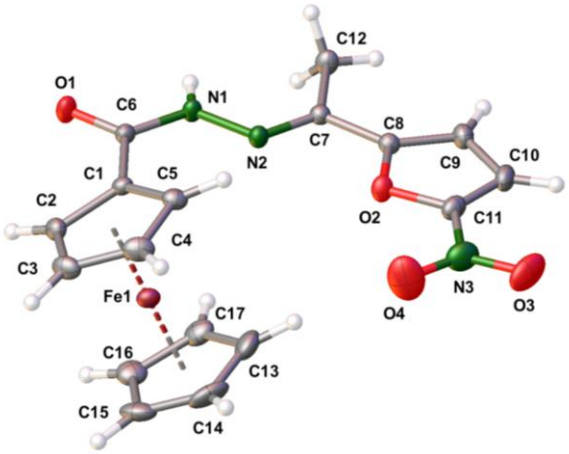

Figure 4. View of the molecular structure of compound **4b** with atomic numbering scheme. Thermal ellipsoids are drawn at 30% probability. Selected bond lengths (Å), bond angles (°), and torsion angles (°): C_5H_4(centroid)–Fe 1.6432(11); C_5H_5(centroid)–Fe 1.6503(14); C(1)–C(6) 1.480(3); C(6)–O(1) 1.232(3); C(6)–N(1) 1.360(3); N(1)–N(2) 1.363(3); N(2)–C(7) 1.284(3); C(7)–C(8) 1.453(3); C(8)–O(2) 1.370(2); C(2)–C(1)–C(6) 120.4(2); C(1)–C(6)–O(1) 120.2(19); C(1)–C(6)–N(1) 121.2(17); C(6)–N(1)–N(2) 120.5(17); N(1)–N(2)–C(7) 118.2(17); N(2)–C(7)–C(8) 115.8(18); C(5)-C(1)-C(6)-O(1) 28.3(2); C(5)-C(1)-C(6)-N(1) 26.8(4); C(6)-N(1)-N(2)-C(7) 1.7(2) and N(2)-C(7)-C(8)-O(2) 3.0(3).

The furyl ring is nearly coplanar with the Cp ring, and their planes form a dihedral angle of 11.5(11)°. The value of torsion angle C(5)-C(1)-C(6)-O(1) [28.3(3)°] supports the preceding observation. The C(6)-N(1) bond length [1.360(3) Å] is smaller than the typical value for a C-N bond (1.469 Å). This could be indicative of the existence of electronic delocalization through the atoms O(1)-C(6)-N(1) [90]. The other bond lengths and angles are in the normal range [73,74].

In the crystal, a molecule sited at (*x*,*y*,*z*) is connected by a proximal one at ($\bar{x}$, $\bar{y}$,1-*z*) by intermolecular N-H···O interactions through an $R_2^2(8)$ graph set motif [93] forming dimers (Table S5 and Fig. S19). As a consequence of the relative arrangement of these structural units in the crystals, the O(3) atom of the two molecules of the dimers is close to the C(17)-H(17) bond of other units belonging to two different vicinal dimers. The distance O(3)···H(17) [2.56(3) Å] is consistent with the existence of weak intermolecular hydrogen bonds [94]. These short contacts result in a 1D chain along the [010] direction.

*3.3. Study of the electrochemical properties of N-acylhydrazones (**4a**,**b** and **5a**,**b**)*

We studied the electrochemical properties of the compounds (**4a**,**b** and **5a**,**b**) at room temperature by cyclic voltammetry in DMSO solutions. When CVs were registered at 0.10 Vs^{-1} (Fig. 5), three cathodic peaks were detected in the range $-1.7\ V < E_c < -0.8\ V$. These peaks were rather broad, especially for **4b**, and this precluded to determine their position with accuracy. In the reverse scan, the resolution of the CV was even lower. However, when the scan rate was increased gradually from 0.1 to 2.0 Vs^{-1}, the quality of the voltammograms improved considerably for all compounds, as shown in Fig. 6 for **4a** (in Figs S20 – S22 for **4b**, **5a**, and **5b**). A summary of the electrochemical data obtained at 2.0 Vs^{-1} is presented in Table 1.

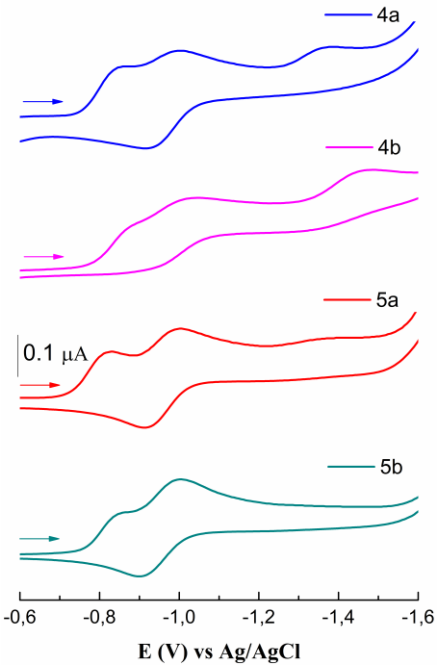

Figure 5. Cyclic voltammograms for all compounds at 0.10 Vs^{-1} DMSO (TBAP 0.1 M, HMDE, Pt, non-aqueous Ag/AgCl).

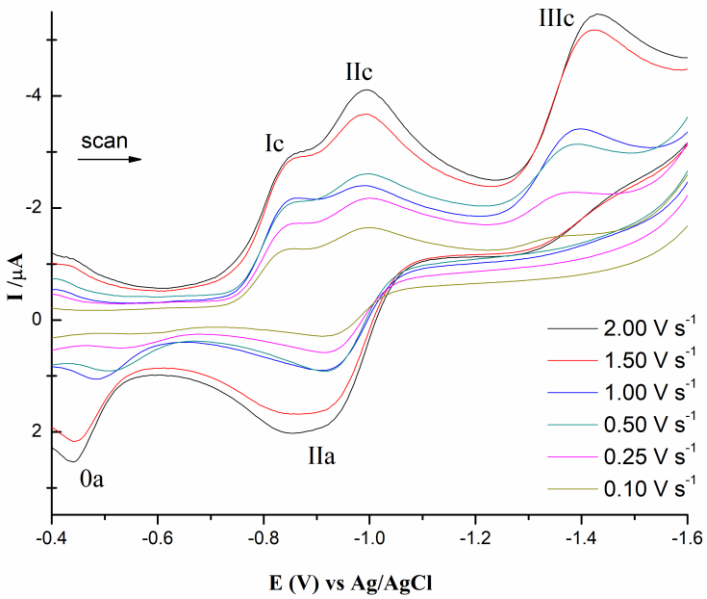

Figure 6. Cyclic voltammogram of compound **4a** at different scan rates varying from 0.1 – 2.00 Vs^{-1} in DMSO (TBAP 0.1 M, HMDE, Pt, non-aqueous Ag/AgCl).

Table 1. Relevant electrochemical data for the organometallic *N*-acylhydrazones and for the drug nifurtimox[a]

	$E_{(p0a)}$	$E_{(pIc)}$	$E_{(pIa)}$	$E_{(pIIc)}$	$E_{(pIIa)}$	$E_{(pIIIc)}$	ΔE[b]	$E_{1/2}$[c]
4a	-0.44	-0.85	–	-0.99	-0.87	-1.43	0.12	-0.93
4b	-0.44	-0.86	–	-1.03	-0.90	-1.50	0.13	-0.97
5a	-0.33	-0.81	–	-0.99	-0.92	-1.39	0.07	-0.96
5b	-0.53	-0.84	–	-1.01	-1.12	-1.70	0.11	-1.07
Nfx		-0.75	-0.70				0.05	-0.73

[a] Measured in DMSO at a scan rate of 2.0 Vs^{-1} [V vs non-aqueous Ag/AgCl(sat)].

[b] $\Delta E = E_{pc} - E_{pa}$ (V).

[c] $E_{1/2} = (E_{pc} + E_{pa})/2$ (V).

The comparison of results reveals that the compounds (**4a**,**b** and **5a**,**b**) exhibit similar electrochemical behaviors. Their CVs showed three peaks (Fig. 6 and Figs. S20 – S22). The first reduction peak (labeled as I_c) was observed at around –0.84 V, and it was attributed to the irreversible one-electron reduction of the group NO_2 to generate the nitro anion radical, shown in the following equation:

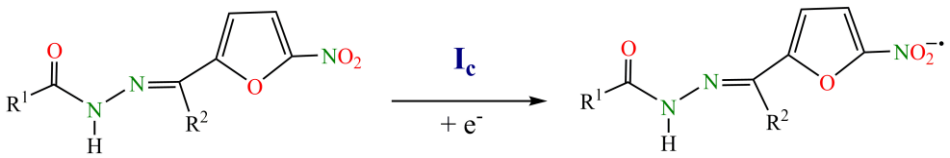

The incorporation of the fragment [-CO-NH-] between the organometallic rings and the 5-nitrofuryl modifies the potential of this step (≈ –0.84 V). Higher reduction potentials (between

–0.6 and –0.7 V) have been observed for analogous complexes, where the organometallic unit joins to heterocycle fragment through a bridge [-N=C-] [66]. The difference in the reduction potential (I_c) indicates that these acylhydrazones have a lower ability to generate nitro anion-radical species, which could have effects on its bioactivation in biological media.

The nitro anion radical formed in this first stage can undergo a multi-step reduction to generate the corresponding hydroxylamine finally. This may occur through different paths depending on the nature of the initial nitro compounds and the reaction media [95]. Previous electrochemical studies on nitro compounds derived from thiosemicarbazones, carbamates, and quinoxaline with fragments prone to undergo deprotonation, have postulated that after the reduction of the NO_2 group of the initial compound, the nitro anion radical formed may be basic enough as to extract an electron from another molecule (known as self-protonation reaction) and generate the protonated and deprotonated species [84,96].

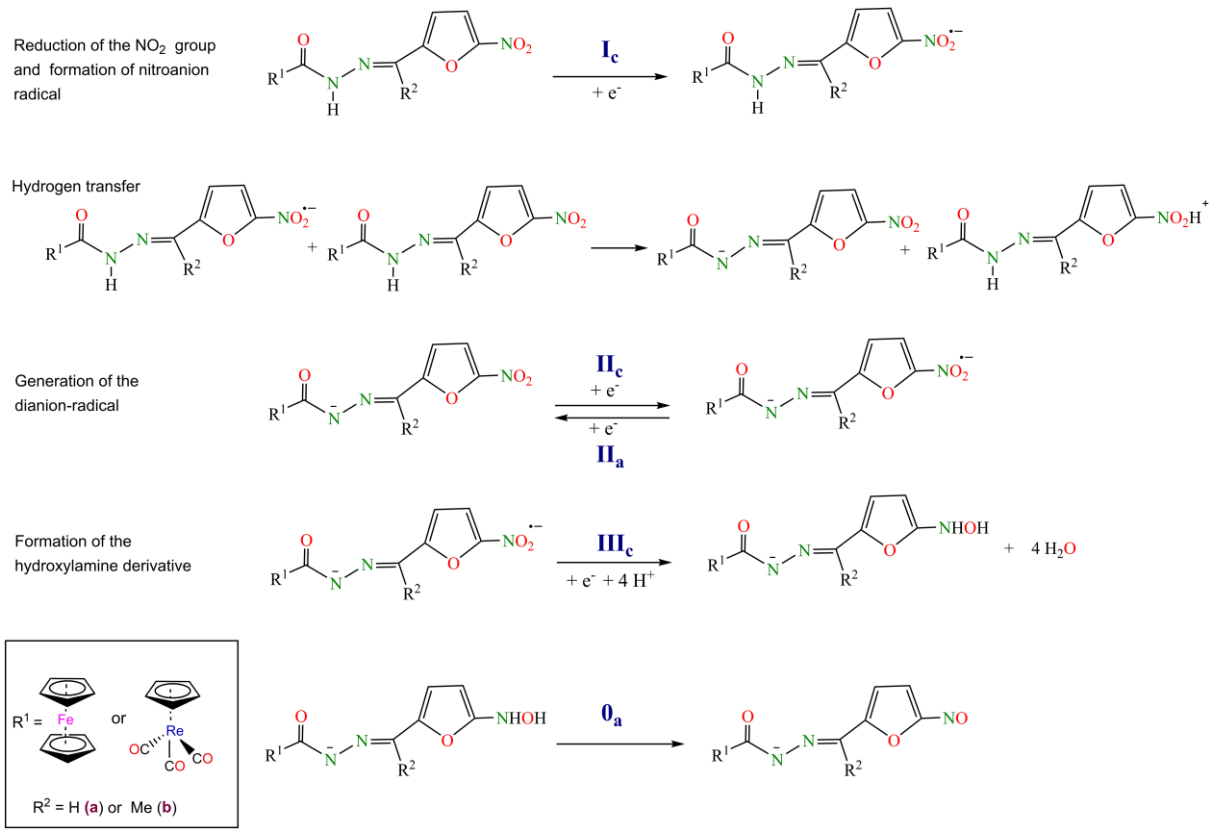

Scheme 2. Proposed self-protonation mechanism for *N*-acylhydrazones **4a**,**b** and **5a**,**b**.

Additional experiments were performed to investigate whether compounds under study also undergo a chemical reaction coupled with the electrochemical process. It is well known that the comparison of the CVs evolution of CVs of freshly prepared compound-solutions and those registered after the successive addition of base aliquots can provide valuable information. Based

on this, and due to the similarity between the electrochemical behavior of the four compounds, we selected complex **4b** as a representative example and compared the CV of the freshly prepared solution with those registered after the addition of NaOH (0.1 M) at a scan rate of 2.0 Vs^{-1}. The results presented in Fig. S23 reveal that upon the addition of the base, the current intensity of the first peaks I_c/I_a decreases, and that of the second pair increases. Thus, a labile proton from a new acylhydrazone molecule is transferred to the nitro anion radical –generated in the first stage– forming the protonated nitro radical and the deprotonated derivative (process identified as hydrogen transfer). The self-protonation mechanism proposed here is illustrated in Scheme 2. This trend is similar to those reported for other nitro-derivatives for which the hydrogen transfer step has been proposed [84,97]

The next couple II_c/II_a, observed in the range –0.87 to –1.12 V, corresponds to the electrochemical reduction of the deprotonated derivative –species formed in the self-protonation reaction– with the consequent formation of the dianion radical. The third peak at ca. –1.51 V (III_c) is assigned –according to the bibliography– to the production of hydroxylamine derivative [63,65,68]. Besides, the CVs exhibit an anodic peak in the range –0.33 and –0.53 V (labelled as 0_a), attributed to the re-oxidation process of hydroxylamine to the nitroso derivative [84].

Moreover, we calculated the half-wave reduction potentials ($E_{1/2}$), which are included in Table 1. The *N*-acylhydrazones **4a**,**b** and **5a**,**b** exhibited more cathodic half-wave reduction potentials ($E_{1/2} \approx -0.98$ V) than the Nfx (–0.73 V). The acylhydrazone linker (-CO-NH-N=C-) is probably associated with the similarity in the $E_{1/2}$ values between the complexes, which would prevent an effective conjugation through the molecule, blocking electronic communication between the two rings and hindering the reduction of the nitro group due to its electron-withdrawing effects. In previous reports, we have observed that the imines containing an alkyl group between the organometallic moiety and the [-N=CH-] bridge exhibit close reduction potentials values [–0.75 and –0.74 V for {R^1-CH_2-N=CH-(5 nitrofuryl)} with R^1 = ferrocenyl or cyrhetrenyl, respectively and –0.68 and –0.65 V for their 5-nitrothienyl partners] [66]. Besides, several thiosemicarbazones and carbamates also based on nitrofuran have shown similar behavior between each series [84,98].

Additionally, small variations in the $E_{1/2}$ values could influence the compound's biological activity and, in particular, the antiparasitic one, since a correlation between the potential values ($E_{1/2}$) of nitro-compounds and their efficiency as trypanocidal agents has been reported. We will return to this point later on.

3.4. Biological results

3.4.1. Antiparasitic activity

It is a well-documented fact that organometallic scaffolds are excellent candidates for developing new drugs, although only a limited number of them have been evaluated as chemotherapeutic agents targeting neglected tropical diseases [33,54,58,61,62]. Because of this, we decided to explore the antiparasitic activities of the complexes (**4a**,**b** and **5a**,**b**) against *T. cruzi* and *T. brucei* and compared their effectiveness to that of the control prodrug, Nfx (Table 2 and Figure 7).

Table 2. Susceptibility of *T. cruzi* epimastigotes, *T. brucei* trypomastigotes, and mammalian cells (L_6) towards organometallic *N*-acylhydrazones and drug nifurtimox.

		EC_{50} (μM)[a] ± SE[b] for:			Selectivity Index[c]	
	R	***T. cruzi***	***T. brucei***	**L_6**	**L_6/*T. cruzi***	**L_6/*T. brucei***
4a	H	11.2 ± 0.49	2.42 ± 0.08	64.86 ± 5.11	5.80	26.8
4b	Me	4.98 ± 0.17	5.08 ± 0.38	26.68 ± 0.81	5.36	5.25
5a	H	3.54 ± 0.13	0.78 ± 0.02	24.34 ± 3.27	6.88	31.2
5b	Me	2.76 ± 0.50	0.28 ± 0.01	<6.25	>2.26	>22.3
Nfx		4.22 ± 0.17	3.56 ± 0.16	88.7 ± 3.49	21.0	24.9

[a] EC_{50}: concentration that inhibits 50% of growth. Values shown are the average of four or more experiments.

[b] SE: standard error.

[c] The Selectivity Index (SI) was calculated as a ratio of the EC_{50} value against L_6 cells to the EC_{50} value against the parasite.

All tested acylhydrazones are active against *T. cruzi* epimastigotes with EC_{50} values ranging from 2.76 to 11.2 μM. Even though the complex **4a** is approximately 3-times less active than Nfx (4.22 μM), the derivatives **4b** (4.98 μM) and **5a** (3.54 μM) exhibit an interesting activity comparable to the standard drug. While the ferrocenyl analog **5b** with an EC_{50} of 2.76 μM turned out to be the best anti-*T. cruzi* agent of the series compounds. The antichagasic potency increases according to the following sequence **4a** < **4b** < Nfx < **5a** < **5b**, indicating that the nature of the organometallic array modifies the activity of these compounds, being the Re(I) derivatives (**5a**,**b**) more potent than their ferrocenyl counterpart (**4a**,**b**). The introduction of a methyl group into iminic carbon (**4b** = 4.98 μM, and **5b** = 2.76 μM) has a slight influence on the biological properties when compared respectively with analogs **4a** (11.2 μM) and **5a** (3.54 μM).

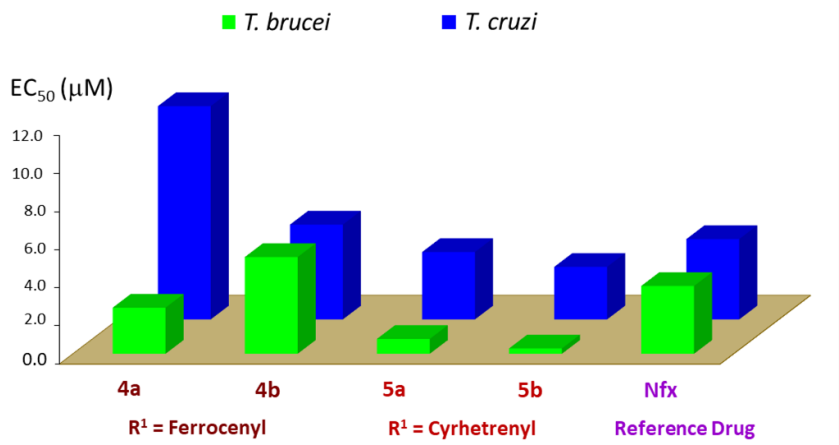

Figure 7. A comparative plot of the EC_{50} values (μM) of ferrocenyl (**4a**,**b**), and cyrhetrenyl (**5a**,**b**) *N*-acylhydrazones, and Nfx against the *T. cruzi* epimastigotes and *T. brucei* trypomastigotes.

The four compounds display activity against *T. brucei*, according to the following sequence **4b** < Nfx < **4a** < **5a** < **5b**, evidencing a similar trend to that observed in the evaluation against *T. cruzi*. Thus, this confirms that organometallic fragments perform an important role in biological activities, being cyrhetrenyl complexes more active than ferrocenyl analogs. Ferrocenyl derivative **4a** shows a significant activity (EC_{50} = 2.42 μM), and cyrhetrenyl analogs **5a** and **5b** with EC_{50} values in the submicromolar range (0.78 and 0.28 μM, respectively) are 4.5- and 13-fold more potent anti-*T. brucei* agents, respectively, in comparison with Nfx. The structure-activity relationship of the imine linker reveals no significant difference in the activity anti-*T. brucei* when a methyl group is incorporated into the iminic carbon (EC_{50} = 2.42 and 0.78 μM for **4a** and **5a**, respectively, versus 5.08 (for **4b**) and 0.28 μM (for **5b**) [67]. However, more derivatives are required to determine the relevance of the R group of [N=C(R)] unit in the biological response and, therefore, in the design of other bioorganometallic compounds.

Based on the results obtained from these *in vitro* studies, it can be seen that all organometallic *N*-acylhydrazones display growth inhibitory properties against both the tested parasite species, with *T. brucei* generally being more sensitive than *T. cruzi*. *T. brucei* is shown to be 4-times more susceptible than *T. cruzi* to **4a** and **5a**; a 10-fold difference in sensitivity is noted towards **5b** while the two trypanosomal species are equally susceptible to **4b** and the control Nfx. In addition, it has been suggested that the Nfx –and 5-nitrofuran derivatives– mediated their cytotoxic activity through induction of oxidative stress in reactions catalyzed by type II NTRs [35,99]. This process begins with the bioreduction of the nitro group to form a nitro anion radical that stimulates the production of superoxide anions and, subsequently, induces oxidative stress in the target cell. In this sense, the NO_2 reduction potential (NO_2 to $NO_2^{\bullet -}$) could predict

how easy this *in vitro* reduction process would be. According to our electrochemical results (described above), the reduction potential ($E_{1/2}$) does not directly correlate to antiparasitic activity (EC_{50}) (Table 1 and 2), suggesting a lower capacity to generate toxic radical species for the parasite from the one-electron transfer process. In this context, these complexes (**4**-**5a**,**b**) could use more than one mechanism to mediate their cytotoxic effects. Several trypanosomal enzymes have been implicated in the metabolism of nifurtimox through 2 electrons reduction, including Type I NTR [20,100]. We will return to this point later on.

It is well known that in new therapeutic agent's design and development, the potency of the drugs or prodrugs is essential. Still, other more subtle factors, i.e. their effect on normal cells selectivity and ADMET properties, among others, should also be considered. In view of this, we also studied ferrocenyl/cyrhetrenyl compounds (**4a**,**b** and **5a**,**b**) on rat skeletal cells L_6, with all of them tested displaying cytotoxicity (Table 2). The cells L_6 are standard mammalian lines commonly used as host cells for *T. cruzi* [9]. The Selectivity Index (SI) (calculated as a ratio of EC_{50} against the mammalian line relative to the EC_{50} against parasite) was determined as an indication of each agent selectivity.

In this regard, the compound **4a** is the less cytotoxic of the series and shows a moderate selectivity ($EC_{50}L_6$ = 64.9 μM, SI = 26.8) towards the *T. brucei* with respect to the parent nifurtimox ($EC_{50}L_6$ = 88.7 μM and SI = 24.9). Although the cyrhetrenyl derivatives **5a** and **5b** are more toxic to L_6 cell than the Nfx, their trypanocidal potency (EC_{50} = 0.78 and 0.28 μM, respectively) and their moderate selectivity (SI = 31.2 and >22.3, respectively) towards the *T. brucei*, compared with the nifurtimox (EC_{50} = 4.22 μM), enhance the potential interest of these two compounds towards the parasite.

*3.4.2. Additional studies to elucidate the action mechanism of N-acylhydrazones (**4b** and **5b**)*

In *T. brucei*, many nitroheterocycles must undergo activation before mediating their trypanocidal effects, a reaction catalyzed by the type I nitroreductase TbNTR1. To test whether this extends to the cyrhetrenyl/ferrocenyl complexes reported here, the susceptibility of BSF trypanosomes induced to overexpress this enzyme was investigated (Table 3). The ratio between –tet and +tet values determines if nitrofurans were metabolized by TbNTR1 in the parasite itself. For **4b** and **5b**, parasites with elevated levels of TbNTR1 (+tet) were shown to be 30- and 15-fold more sensitive to the metallorganic compound than controls (–tet), respectively. This phenotype was shown to be structure dependent as cells overexpressing this

nitroreductase had the same susceptibility as controls to the non-nitroheterocyclic compound MelB (see comparative Figure S24 in ESI).

Based on these results and as has been observed for other nitroheterocycles [38,67], we suggest that the predominant reaction of the nitrofuryl acylhydrazones catalyzed by TbNTR1 leads to the opening of the furan ring to form unsaturated and then saturated open-chain nitriles [35]. The unsaturated form can function as a Michael acceptor and could react non-specifically with various cellular components. This may then target several unrelated pathways/systems and is believed to account for the multiple effects nifurtimox has on trypanosomes, where treatment has been reported to inhibit various enzyme activities, modify thiol levels, and cause DNA damage [101,102].

Table 3. Susceptibilities of *T. brucei* bloodstream-form trypomastigotes with elevated levels of TbNTR1 to organometallic *N*-acylhydrazones[a].

	***T. brucei* EC_{50} (μM)[b]**		**Ratio**
	TbNTR1 (–tet)	**TbNTR1 (+tet)**	**–tet/+tet**
4b	5.70 ± 0.21	0.19 ± 0.01	30
5b	0.30 ± 0.02	0.02 ± 0.00	15
Nfx[c]	3.00 ± 0.22	0.27 ± 0.03	11
MelB[c,d]	4.0 ± 0.1	3.4 ± 0.1	1

[a] Growth-inhibitory effect as judged by the EC_{50} values (in μM) of all nitrofuran compounds on *T. brucei* bloodstream-form control (–tet) and TbNTR1-overexpressing (+tet) cells.

[b] Data shown are means over four experiments ± standard deviations.

[c] Nifurtimox (Nfx) and melarsoprol (MelB) were used as control drugs.

[d] EC_{50} values for MelB are in nM.

4. Conclusion

Four ferrocenyl/cyrhetrenyl complexes of general formula [R^1-C(O)-NH-N=C(R^2)(5-nitrofuryl)] with [R^1 = ferrocenyl (**4**) or cyrhetrenyl (**5**); and R^2 = H (**a**) or Me (**b**)], were synthesized and characterized in the solid-state and solution. Electrochemical studies revealed that acylhydrazones involve a self-protonation process, and reduction potentials ($E_{1/2}$) of the Ar-NO_2 group were close to –0.98 V are more prone to reduction than Nfx ($E_{1/2}$ = –0.73 V).

The results obtained from the biological studies demonstrate that the *N*-acylhydrazones were active *in vitro* against both parasites, exhibiting a higher level of potency towards *T. brucei* with respect to *T. cruzi*. The ferrocenyl analog **4a**, with equivalent activity to the Nfx, showed moderate toxicity and selectivity concerning the selected mammalian cell model, being the most

successful anti-HAT agent. Cyrhetrenyl derivatives **5a** and **5b** proved had low EC_{50} values (0.78 and 0.28 μM, respectively) along with moderate selectivity to *T. brucei* (31.2 and >22.3, respectively), although they were toxic against L_6 cells. *N*-acylhydrazones **4b** and **5b** induced elevated levels of TbNTR1 (+tet) in trypanosomes, up to 30- and 15-fold more sensitive to organometallic compound than controls (–tet), indicating that both acylhydrazones are a substrate for TbNTR1 (–tet/+tet) within the parasite.

In conclusion, we have proved that the compounds **4a**,**b** and **5a**,**b** have high stability (in the solid-state and solution), exhibit interesting redox properties, outstanding anti-CD, and anti-HAT activities (moderate or low) toxicity L_6 cells and, are capable of targeting type I NTR. These findings, together with the presence of the organometallic array, the *N*-acylhydrazone bridge, and the 5-nitrofuryl unit in the single small molecules of **4a**,**b** and **5a**,**b** –especially of **5a** and **5b** due to their higher stability in solution at 37 °C– have an added value and open up a wide range of further studies. Including not only the investigation of their potential antiparasitic activity against other diseases with high incidence like leishmaniasis, where the NTR also play an essential role; or trichomoniasis, one of the most common sexually transmitted diseases worldwide caused by the *Trichomonas vaginalis* parasite; but also, other biological activities, typically displayed by nitro-based drugs and especially those holding 5-nitrofuryl cores. Finally, it should be noted that the structures of the compounds can be developed to generate new nitroheterocycle-based prodrug treatments that exploit activation mechanisms that are present in and essential to the parasite with such activities absent from the mammalian host.

Acknowledgments

P.M.T. would like to thank to postdoctoral FONDECYT grant 3200273. C.L. is also grateful to the *Ministerio de Economía y Competitividad* of Spain for financial support [Grant n. CTQ-2015-65040P (subprogram BQU)].

Appendix A. Supplementary data

CCDC 2039709 – 2039710 contains the supplementary crystallographic data for this paper. These data can be obtained free of charge from the Cambridge Crystallographic Data Centre, 12 Union Road, Cambridge CB2 1EZ, UK; fax: (+44) 1223-336-033; or e-mail: deposit@ccdc.cam.ac.uk.

ABBREVIATIONS

ADMET: Absorption, Distribution, Metabolism, Excretion and Toxicity

BSF: bloodstream form

CD: Chagas disease

CV: Cyclic voltammogram

DMSO: Dimethylsulfoxide

$E_{1/2}$: Half-wave reduction potential

EC_{50}: Half maximal effective concentration

EI-MS: Electron impact mass spectra

FT-IR: Fourier-transformed infrared spectroscopy

HAT: Human African Trypanosomiasis

HEPES: 4-(2-hydroxyethyl)-1-piperazineethanesulfonic acid

HMDE: Hanging mercury drop electrode

MELB: Melarsoprol

NAH: *N*-acylhydrazone

NFX: Nifurtimox

NMR: Nuclear magnetic resonance

NTR: Nitroreductase

RPMI: Roswell Park Memorial Institute medium

SI: Selectivity index

TBAP: Tetrabutylammonium perchlorate

TET: Tetracycline

THF: Tetrahydrofuran

UV-Vis: Ultraviolet-visible

References

[1] WHO. Chagas Disease. https://www.who.int/health-topics/chagas-disease#tab=tab_1, 2020 (Accessed 28 December 2020).

[2] WHO. Trypanosomiasis, human African. https://www.who.int/news-room/fact-sheets/detail/trypanosomiasis-human-african-(sleeping-sickness), 2020 (Accessed 28 December 2020).

[3] V. Nissapatorn, H. S. Oz (Eds.), Chagas disease: Basic investigation and Challenges, Intechopen (2018).

[4] J. A. Pérez-Molina, I. Molina, Chagas disease, Lancet 391 (2018) 82–94. https://doi.org/10.1016/S0140-6736(17)31612-4.

[5] P. Büscher, G. Cecchi, V. Jamonneau, G. Priotto, Human African trypanosomiasis, Lancet 390 (2017) 2397–2409. https://doi.org/10.1016/S0140-6736(17)31510-6.

[6] L. Makhani, A. Khatib, A. Corbeil, R. Kariyawasam, H. Raheel, S. Clarke, P. Challa, E. Hagopian, S. Chakrabarti, K. L. Schwartz, A. K. Boggild, 2018 in review: five hot topics in tropical medicine, Trop. Dis. Travel Med. Vaccines, 5 (2019) 5. https://doi.org/10.1186/s40794-019-0082-z.

[7] H. P. De Koning, The drugs for sleeping sickness: their mechanism of action and resistance and a brief history, Trop. Med. Infect. Dis. 5 (2020) 14. https://doi.org/10.3390/tropicalmed5010014.

[8] A. F. Francisco, S. Jayawardhana, F. Olmo, M. D. Lewis, S. R. Wilkinson, M. C. Taylor, J. M. Kelly, Challenges in Chagas disease drug development, Molecules 25 (2020) 2799. https://doi.org/10.3390/molecules25122799.

[9] C. H. Franco, L. M. Alcântara, E. Chatelain, L. Freitas-Junior, C. Borsoi Moraes, Drug discovery for chagas disease: Impact of different host cell lines on assay performance and hit compound selection, Trop. Med. Infect. Dis. 4 (2019) 82. https://doi.org/10.3390/tropicalmed4020082.

[10] W. H. Kawaguchi, L. B. Cerqueira, M. Millan Fachi, M. L. Campos, I. J. M. Reason, R. Pontarolo, Efficacy and Safety of Chagas Disease Drug Therapy and Treatment Perspectives, in: V. Nissapatorn (ed.), Chagas disease: Basic investigation and Challenges, 2018, pp. 381. https://doi.org/10.5772/intechopen.74845.

[11] S. Patterson, A. H. Fairlamb, Current and future prospects of nitro-compounds as drugs for trypanosomiasis and leishmaniasis, Curr. Med. Chem. 26 (2019) 4454–4475. https://doi.org/10.2174/0929867325666180426164352.

[12] Drug.com, Nifurtimox (Systemic). https://www.drugs.com/mmx/nifurtimox.html, 2020 (Accessed 28 December 2020).

[13] A. M. Mejia, B. S. Hall, M. C. Taylor, A. Gómez-Palacio, S. R. Wilkinson, O. Triana-Chávez, J. M. Kelly, Benznidazole-resistance in trypanosoma cruzi is a readily acquired trait that can arise independently in a single population, J. Infect. Dis. 206 (2012) 220–228. https://doi.org/10.1093/infdis/jis331.

[14] B. Enanga, M. R. Ariyanayagam, M. L. Stewart, M. P. Barrett, Activity of megazol, a trypanocidal nitroimidazole, is associated with DNA damage, Antimicrob. Agents Chemother. 47 (2003) 3368–3370. https://doi.org/10.1128/AAC.47.10.3368-3370.2003.

[15] E. T. Ryan, D. R. Hill, T. Solomon, N. E. Aronson, T. P. Endy (Eds.), Hunter's Tropical Medicine and Emerging Infectious Diseases, 10th Ed., Elsevier, 2020.

[16] A. H. Fairlamb, D. Horn, Melarsoprol resistance in African trypanosomiasis, Trends Parasitol. 34 (2018) 481–492. https://doi.org/10.1016/j.pt.2018.04.002.

[17] O. Yun, G. Priotto, J. Tong, L. Flevaud, F. Chappuis, 2010. NECT Is next: Implementing the new drug combination therapy for *trypanosoma brucei gambiense* sleeping sickness. PLoS Negl. Trop. Dis. 4, e720. https://doi.org/10.1371/journal.pntd.0000720.

[18] E. D. Deeks, Fexinidazole: First global approval, Drugs 79 (2019) 215–220. https://doi.org/10.1007/s40265-019-1051-6.

[19] C. J. Forsyth, S. Hernández, W. Olmedo, A. Abuhamidah, M. I. Traina, D. R. Sanchez, J. Soverow, S. K. Meymandi, Safety profile of nifurtimox for treatment of Chagas disease in the United States, Clin. Infect. Dis. 63 (2016) 1056–1062. https://doi.org/10.1093/cid/ciw477.

[20] S. R. Wilkinson, M. C. Taylor, D. Horn, J. M. Kelly, I. Cheeseman, A mechanism for cross-resistance to nifurtimox and benznidazole in trypanosomes, Proc. Natl. Acad. Sci. U.S.A. 105 (2008) 5022–5027. https://doi.org/10.1073/pnas.0711014105.

[21] M. Decker (ed), Hybrid Molecules for Drugs Development, 1st Edition, Elsevier, Würzburg, Germany, 2017.

[22] L. Yet, Privileged Structures in Drug Discovery: Medicinal Chemistry and Synthesis, John Wiley & Sons, 2018.

[23] R. Matsa, P. Makam, M. Kaushik, S. L. Hoti, T. Kannan, 2019. Thiosemicarbazone derivatives: Design, synthesis and *in vitro* antimalarial activity studies. Eur. J. Pharm. Sci. 137, 104986. https://doi.org/10.1016/j.ejps.2019.104986.

[24] K. Figarella, S. Marsiccobetre, I. Galindo-Castro, N. Urdaneta, J. C. Herrera, N. Canudas, E. Galarraga, Antileishmanial and antitrypanosomal activity of synthesized hydrazones, pyrazoles, pyrazolo[1,5-a]-pyrimidines and pyrazolo[3,4-b]-pyridine, Curr. Bioact. Compd. 14 (2018) 234–239. https://doi.org/10.2174/1573407213666170405121810.

[25] N. N. Santiago, G. P. de Alcântara, J. S. da Costa, S. A. Carvalho, J. M. C. Barbosa, K. Salomão, S. L. de Castro, H. M. G. Pereira, E. F. da Silva, Synthesis and antitrypanosomal profile of novel hydrazonoyl derivatives, Med. Chem. 16 (2020) 487–494. https://doi.org/10.2174/1573406415666190712115237.

[26] N. Le Dang, T. B. Hughes, G. P. Miller, S. J. Swamidass, Computational approach to structural alerts: furans, phenols, nitroaromatics, and thiophenes, Chem. Res. Toxicol. 30 (2017) 1046–1059. https://doi.org/10.1021/acs.chemrestox.6b00336.

[27] S. Thota, D. A. Rodrigues, P. de Sena Murteira Pinheiro, L. M. Lima, C. A. M. Fraga, E. J. Barreiro, *N*-acylhydrazones as drugs, Bioorg. Med. Chem. Lett. 28 (2018) 2797–2806. https://doi.org/10.1016/j.bmcl.2018.07.015.

[28] K. Nepali, H.-Y. Lee, J.-P. Liou, Nitro-group-containing drugs, J. Med. Chem. 6 (2019) 2851–2893. https://doi.org/10.1021/acs.jmedchem.8b00147.

[29] L. Ronconi, P. J. Sadler, Using coordination chemistry to design new medicines, Coord. Chem. Rev. 251 (2007) 1633–1648. https://doi.org/10.1016/j.ccr.2006.11.017.

[30] R. K. Sodhi, S. Paul, 2019. Metal complexes in medicine: An overview and update from drug design perspective. Canc. Therapy Oncol. Int. J. 14, 555883. https://doi.org/10.19080/CTOIJ.2019.13.555883.

[31] L. Riccardi, V. Genna, M. de Vivo, Metal–ligand interactions in drug design, Nat. Rev. Chem. 2 (2018) 100–112. https://doi.org/10.1038/s41570-018-0018-6.

[32] A. Chylewska, M. Biedulska, P. Sumczynski, M. Makowski, Metallopharmaceuticals in therapy - A new horizon for scientific research, Curr. Med. Chem. 25 (2018) 1729–1791. https://doi.org/10.2174/0929867325666171206102501.

[33] R. W. Brown, C. J. T. Hyland, Medicinal organometallic chemistry – an emerging strategy for the treatment of neglected tropical diseases, Med. Chem. Commun. 6 (2015) 1230–1243. https://doi.org/10.1039/C5MD00174A.

[34] H. A. Zhong, ADMET Properties: Overview and Current Topics, in: A. Grover (Ed.), Drug Design Principles and Applications, Springer, 2017, pp. 113.

[35] B. S. Hall, C. Bot, S. R. Wilkinson, Nifurtimox activation by trypanosomal type I nitroreductases generates cytotoxic nitrile metabolites, J. Biol. Chem. 286 (2011) 13088–13095. https://doi.org/10.1074/jbc.M111.230847.

[36] C. Olea-Azar, A. M. Atria, R. di Maio, G. Seoane, H. Cerecetto, Electron spin resonance and cyclic voltammetry studies of nitrofurane and nitrothiophene analogues of nifurtimox, Spectrosc. Lett. 31 (1998) 849–857. https://doi.org/10.1080/00387019808007403.

[37] C. Gallardo-Garrido, Y. Cho, J. Cortés-Rios, D. Vásquez, C. D. Pessoa-Mahana, R. Araya-Maturana, H. Pessoa-Mahana, M. Faundez, 2020. Nitrofuran drugs beyond redox cycling: Evidence of nitroreduction-independent cytotoxicity mechanism. Toxicol. Appl. Pharmacol. 401, 115104. https://doi.org/10.1016/j.taap.2020.115104.

[38] C. Bot, B. S. Hall, G. Álvarez, R. Di Maio, M. González, H. Cerecetto, S. R. Wilkinson, Evaluating 5-nitrofurans as trypanocidal agents, Antimicrob. Agents Chemother. 57 (2013) 1638–1647. https://doi.org/10.1128/AAC.02046-12.

[39] C. Barrientos-Salcedo, B. Espinoza, C. Soriano-Correa, Computational study of substituent effects on the physicochemical properties of selected antiparasitic 5-nitrofuran, J. Mol. Struct. 1173 (2018) 92–99. https://doi.org/10.1016/j.molstruc.2018.06.089.

[40] L. Campos-Fernández, C. Barrientos-Salcedo, E. E. Herrera Valencia, R. Ortiz-Muñiz, C. Soriano-Correa, Substituent effects on the stability, physicochemical properties and chemical reactivity of nitroimidazole derivatives with potential antiparasitic effect: a computational study, New J. Chem. 43 (2019) 1125–1134. https://doi.org/10.1039/c9nj02207d.

[41] L. N. F. Cardoso, T. C. M. Nogueira, F. A. R. Rodrigues, A. C. Aragão Oliveira, M. C. dos Santos Luciano, C. Pessoa, M. V. N. de Souza, *N*-acylhydrazones containing thiophene nucleus: a new anticancer class, Med. Chem. Res. 26 (2017) 1605–1608. https://doi.org/10.1007/s00044-017-1832-y.

[42] W. C. Souza, L. D. Dias, J. E. de Queiroz, H. D. A. Vidal, V. B. da Silva, A. M. Leopoldino, C. H. T. de Paula da Silva, G. M. V. Verde, G. L. B. Aquino, *N*-acylhydrazones derivatives as novel ligands against cancer in inhibition of interaction

between nucleic acids and hnRNP K protein, Curr. Bioact. Compd. 16 (2020) 432–441. https://doi.org/10.2174/1573407215666190131121059.

[43] A. M. F. Rozada, F. A. V. Rodrigues-Vendramini, D. S. Gonçalves, F. A. Rosa, E. A. Basso, F. A. V. Seixas, É. S. Kioshima, G. F. Gauze, 2020. Synthesis and antifungal activity of new hybrids pyrimido[4,5-*d*]pyridazinone-*N*-acylhydrazones. Bioorg. Med. Chem. Lett. 30, 127244. https://doi.org/10.1016/j.bmcl.2020.127244.

[44] C. Lazzarini, K. Haranahalli, R. Rieger, H. K. Ananthula, P. B. Desai, A. Ashbaugh, M. J. Linke, M. T. Cushion, B. Ruzsicska, J. Haley, I. Ojima, M. Del Poeta, 2018. Acylhydrazones as antifungal agents targeting the synthesis of fungal sphingolipids. Antimicrob. Agents Chemother. 62, e00156. https://doi.org/10.1128/AAC.00156-18.

[45] D. G. G. Rando, M. O. L. da Costa, T. F. A. Pavani, T. Oliveira, P. F. Dos Santos, C. R. Amorim, P. L. S. Pinto, M. G. de Brito, M. P. N. Silva, D. B. Roquini, J. de Moraes, Vanillin-related *N*-acylhydrazones: Synthesis, antischistosomal properties and target fishing studies, Curr. Top. Med. Chem. 19 (2019) 1241–1251. https://doi.org/10.2174/1568026619666190620163237.

[46] E. Bettiol, M. Samanovic, A. S. Murkin, J. Raper, F. Buckner, A. Rodriguez, 2009. Identification of three classes of heteroaromatic compounds with activity against intracellular *Trypanosoma cruzi* by chemical library screening. Plos Negl. Trop. Dis. 3, e384. https://doi.org/10.1371/journal.pntd.0000384.

[47] S. A. Carvalho, L. O. Feitosa, M. Soares, T. E. M. M. Costa, M. G. Henriques, K. Salomão, S. L. de Castro, M. Kaiser, R. Brun, J. L. Wardell, S. M. S. V. Wardell, G. H. G. Trossini, A. D. Andricopulo, E. F. da Silva, C. A. M. Fraga, Design and synthesis of new (*E*)-cinnamic *N*-acylhydrazones as potent antitrypanosomal agents, Eur. J. Med. Chem. 54 (2012) 512–521. https://doi.org/10.1016/j.ejmech.2012.05.041.

[48] D. R. Guay, An update on the role of nitrofurans in the management of urinary tract infections, Drugs 61 (2001) 353–364. https://doi.org/10.2165/00003495-200161030-00004.

[49] C. C. McOsker, P. M. Fitzpatrick, Nitrofurantoin: mechanism of action and implications for resistance development in common uropathogens, J. Antimicrob. Chemother. 33 (1994) 23–30. https://doi.org/10.1093/jac/33.suppl_a.23.

[50] B. Begovic, S. Ahmedtagic, L. Calkic, M. Vehabović, S. B. Kovacevic, T. Catic, M. Mehic, Open clinical trial on using nifuroxazide compared to probiotics in treating acute

diarrhoeas in adults, Mater Sociomed. 28 (2016) 454–458. https://doi.org/10.5455/msm.2016.28.454-458.

[51] M. S. D Alves, R. N. das Neves, Â. Sena-Lopes, M. Domingues, A. M. Casaril, N. Vieira Segatto, T. C. Mendonça Nogueira, M. V. Nora de Souza, L. Savegnago, F. Kömmling Seixas, T. Collares, S. Borsuk, Antiparasitic activity of furanyl *N*-acylhydrazone derivatives against *Trichomonas vaginalis*: *in vitro* and *in silico* analyses, Parasit. Vectors 13 (2020) 59. https://doi.org/10.1186/s13071-020-3923-8.

[52] L. Otero, M. Vieites, L. Boiani, A. Denicola, C. Rigol, L. Opazo, C. Olea-Azar, J. D. Maya, A. Morello, R. L. Krauth-Siegel, O. E. Piro, E. Castellano, M. González, D. Gambino, H. Cerecetto, Novel antitrypanosomal agents based on palladium nitrofurylthiosemicarbazone complexes: DNA and redox metabolism as potential therapeutic targets, J. Med. Chem. 49 (2006) 3322–3331. https://doi.org/10.1021/jm0512241.

[53] M. Pagano, B. Demoro, J. Toloza, L. Boiani, M. González, H. Cerecetto, C. Olea-Azar, E. Norambuena, D. Gambino, L. Otero, Effect of ruthenium complexation on trypanocidal activity of 5-nitrofuryl containing thiosemicarbazones, Eur. J. Med. Chem. 44 (2009) 4937–4943. https://doi.org/10.1016/j.ejmech.2009.08.008.

[54] E. Rodríguez Arce, I. Machado, B. Rodríguez, M. Lapier, M. C. Zúñiga, J. D. Maya, C. Olea Azar, L. Otero, D. Gambino, Rhenium(I) tricarbonyl compounds of bioactive thiosemicarbazones: Synthesis, characterization and activity against *Trypanosoma cruzi*, J. Inorg. Biochem. 170 (2017) 125–133. https://doi.org/10.1016/j.jinorgbio.2017.01.011.

[55] A. Zülfikaroğlu, Ç. Yüksektepe Ataol, E. Çelikoğlu, U. Çelikoğlu, Ö. İdil, 2020. New Cu(II), Co(III) and Ni(II) metal complexes based on ONO donor tridentate hydrazone: Synthesis, structural characterization, and investigation of some biological properties. J. Mol. Struct. 1199, 127012. https://doi.org/10.1016/j.molstruc.2019.127012.

[56] D. Rogolino, M. Carcelli, A. Bacchi, C. Compari, L. Contardi, E. Fisicaro, A. Gatti, M. Sechi, A. Stevaert, L. Naesens, A versatile salicyl hydrazonic ligand and its metal complexes as antiviral agents, J. Inorg. Biochem. 150 (2015) 9–17. https://doi.org/10.1016/j.jinorgbio.2015.05.013.

[57] G. S. Hegde, S. P. Netalkar, V. K. Revankar, 2019. Copper (II) complexes of 3,5-di-*tert*-butyl-2-hydroxybenzoylhydrazones of 2-formylpyridine and 2-acetylpyridine, with tautomeric azine-scaffold-based architecture: Synthesis, crystal structures, the effect of

counteranions on complexation, and their anti-microbial and anti-tuberculosis evaluation. Appl. Organomet. Chem. 33, e4840. https://doi.org/10.1002/aoc.4840.

[58] M. F. Mosquillo, P. Smircich, M. Ciganda, A. Lima, D. Gambino, B. Garat, L. Pérez-Díaz, Comparative high-throughput analysis of the *Trypanosoma cruzi* response to organometallic compounds, Metallomics 12 (2020) 813–828. https://doi.org/10.1039/D0MT00030B.

[59] M. Cipriani, J. Toloza, L. Bradford, E. Putzu, M. Vieites, E. Curbelo, A. I. Tomaz, B. Garat, J. Guerrero, J. S. Gancheff, J. D. Maya, C. Olea-Azar, D. Gambino, L. Otero, Effect of the metal ion on the anti *T. cruzi* activity and mechanism of action of 5-nitrofuryl-containing thiosemicarbazone metal complexes, Eur. J. Inorg. Chem. (2014) 4677–4689. https://doi.org/10.1002/ejic.201402614.

[60] D. Gambino, L. Otero, Design of prospective antiparasitic metal-based compounds including selected organometallic cores, Inorg. Chim. Acta 472 (2018) 58–75. https://doi.org/10.1016/j.ica.2017.07.068.

[61] F. Rivas, A. Medeiros, E. Rodríguez Arce, M. Comini, C. M. Ribeiro, F. R. Pavan, D. Gambino, New heterobimetallic ferrocenyl derivatives: Evaluation of their potential as prospective agents against trypanosomatid parasites and *Mycobacterium tuberculosis*, J. Inorg. Biochem. 187 (2018) 73–84. https://doi.org/10.1016/j.jinorgbio.2018.07.013.

[62] J. Oyarzo, A. Acuña, H. Klahn, R. Arancibia, C. P. Silva, R. Bosque, C. López, M. Font-Bardía, C. Calvis, R. Messeguer, Isomeric and hybrid ferrocenyl/cyrhetrenyl aldimines: a new family of multifunctional compounds, Dalton Trans. 47 (2018) 1635–1649. https://doi.org/10.1039/C7DT04142J.

[63] P. Toro, C. Suazo, A. Acuña, M. Fuentealba, V. Artigas, R. Arancibia, C. Olea-Azar, M. Moncada, S. Wilkinson, A. H. Klahn, Cyrhetrenylaniline and new organometallic phenylimines derived from 4- and 5-nitrothiophene: Synthesis, characterization, X-Ray structures, electrochemistry and in vitro anti-*T. brucei* activity, J. Organomet. Chem. 862 (2018) 13–21. doi.org/10.1016/j.jorganchem.2018.03.004.

[64] P. M. Toro, A. Acuña, M. Mallea, M. Lapier, M. Moncada-Basualto, J. Cisterna, I. Brito, H. Klahn, 2019. Condensation and substitution products obtained in reactions of isomeric bromo-nitrofuraldehydes with ferrocenylamine: Electrochemistry and anti-parasitic evaluation. J. Organomet. Chem. 901, 120946. https://doi.org/10.1016/j.jorganchem.2019.120946.

[65] R. Arancibia, A. H. Klahn, G. E. Buono-Core, E. Gutierrez-Puebla, A. Monge, M. E. Medina, C. Olea-Azar, J. D. Maya, F. Godoy, Synthesis, characterization and anti-*Trypanosoma cruzi* evaluation of ferrocenyl and cyrhetrenyl imines derived from 5-nitrofurane, J. Organomet. Chem. 696 (2011) 3238–3244. https://doi.org/10.1016/j.jorganchem.2011.06.038.

[66] R. Arancibia, A. H. Klahn, G. E. Buono-Core, D. Contreras, G. Barriga, C. Olea-Azar, M. Lapier, J. D. Maya, A. Ibañez, M. T. Garland, Organometallic Schiff bases derived from 5-nitrothiophene and 5-nitrofurane: Synthesis, crystallographic, electrochemical, ESR and anti *Trypanosoma cruzi* studies, J. Organomet. Chem. 743 (2013) 49–54. https://doi.org/10.1016/j.jorganchem.2013.06.014.

[67] P. M. Toro, J. Oyarzo, R. Arancibia, S. Wilkinson, V. Artigas, M. Fuentealba, M. Moncada-Basualto, C. Olea-Azar, A. Vega, A. H. Klahn, 2021. Comparison of chemical and biological properties of organometallic complexes containing 4- and 5-nitrothienyl groups. Polyhedron, 193, 114872. https://doi.org/10.1016/j.poly.2020.114872.

[68] J. Gómez, A. H. Klahn, M. Fuentealba, D. Sierra, C. Olea-Azar, J. D. Maya, M. E. Medina, Ferrocenyl and cyrhetrenyl azines containing a 5-nitroheterocyclic moiety: Synthesis, structural characterization, electrochemistry and evaluation as anti-*Trypanosoma cruzi* agents, J. Organomet. Chem. 839 (2017) 108–115. doi.org/10.1016/j.jorganchem.2017.03.014.

[69] J. Oyarzo, R. Bosque, P. Toro, C. P. Silva, R. Arancibia, M. Font-Bardía, V. Artigas, C. Calvis, R. Messeguer, A. H. Klahn, C. López, A novel type of organometallic 2-R-2,4-dihydro-1*H*-3,1-benzoxazine with R = [M(η^5-C_5H_4)$(CO)_3$] (M = Re or Mn) units. Experimental and computational studies of the effect of substituent R on ring-chain tautomerism, Dalton Trans. 48 (2019) 1023–1039. https://doi.org/10.1039/C8DT03265C.

[70] C. Concha, C. Quintana, A. H. Klahn, V. Artigas, M. Fuentealba, C. Biot, I. Halloum, L. Kremerc, R. López, J. Romanos, Y. Huentupil, R. Arancibia, Organometallic tosyl hydrazones: Synthesis, characterization, crystal structures and *in vitro* evaluation for anti-*Mycobacterium tuberculosis* and antiproliferative activities, Polyhedron 131 (2017) 40–45. http://dx.doi.org/10.1016/j.poly.2017.04.031.

[71] Y. Huentupil, P. Chung, N. Novoa, R. Arancibia, P. Roussel, J. Oyarzo, A. H. Klahn, C. P. Silva, C. Calvis, R. Messeguer, R. Bosque, C. López, Novel homo-(Fe_2) and heterobimetallic [(Fe,M) with M = Re or Mn] sulfonyl hydrazones, Dalton Trans. 49

(2020) 12249–12265. https://doi.org/10.1039/D0DT01756F.

[72] F. D. Popp, E. B. Moynahan, Ferrocene studies. IV. Some furan containing derivatives of ferrocene, J. Heterocycl. Chem. 7 (1970) 351–354. https://doi.org/10.1002/jhet.5570070216.

[73] J. Zhang, Preparation, characterization, crystal structure and bioactivity determination of ferrocenyl–thiazoleacylhydrazones, Appl. Organomet. Chem. 22 (2008) 6–11. https://doi.org/10.1002/aoc.1338.

[74] V. Tirkey, S. Mishra, H. R. Dash, S. Das, B. P. Nayak, S. M. Mobin, S. Chatterjee, Synthesis, characterization and antibacterial studies of ferrocenyl and cymantrenyl hydrazone compounds, J. Organomet. Chem. 732 (2013) 122–129. https://doi.org/10.1016/j.jorganchem.2013.02.020.

[75] G. M. Maguene, J. Jakhlal, M. Ladyman, A. Vallin, D. A. Ralambomanana, T. Bousquet, J. Maugein, J. Lebibi, L. Pélinski, Synthesis and antimycobacterial activity of a series of ferrocenyl derivatives, Eur. J. Med. Chem. 46 (2011) 31–38. https://doi.org/10.1016/j.ejmech.2010.10.004.

[76] P. Krishnamoorthy, P. Sathyadevi, R. R. Butorac, A. H. Cowley, N. S. P. Bhuvanesh, N. Dharmaraj, Copper(I) and nickel(II) complexes with 1:1 vs. 1:2 coordination of ferrocenyl hydrazone ligands: Do the geometry and composition of complexes affect DNA binding/cleavage, protein binding, antioxidant and cytotoxic activities?, Dalton Trans. 41 (2012) 4423–4436. https://doi.org/10.1039/C2DT11938B.

[77] Y. Huentupil, L. Peña, N. Novoa, E. Berrino, R. Arancibia, C. T. Supuran, New sulfonamides containing organometallic-acylhydrazones: synthesis, characterisation and biological evaluation as inhibitors of human carbonic anhydrases, J. Enzyme Inhib. Med. Chem. 34 (2019) 451–458. https://doi.org/10.1080/14756366.2018.1555156.

[78] W. L. F. Armarego, W. L. F. Armarego, C, Chai, Purification of Laboratory Chemicals, 6th edition, Butterworth–Heinemann, Oxford, UK, 2009.

[79] P. M. Toro, D. H. Jara, A. H. Klahn, D. Villaman, M. Fuentealba, A. Vega, N. Pizarro, Spectroscopic study of the *E*/*Z* photoisomerization of a new cyrhetrenyl acylhydrazone: A potential photoswitch and photosensitizer, Photochem. Photobiol. 97 (2021) 61–70. https://doi.org/10.1111/php.13309.

[80] Bruker AXS INC., APEX3 Package, APEX3, SAINT and SADABS, Bruker AXS Inc., Madison, Wisconsin, USA, 2016.

[81] G. M. Sheldrick, SADABS, Software for Empirical Absorption Correction, Univ.

Göttingen, Ger. (2000) SADABS, Software for Empirical Absorption Correcti.

[82] G. M. Sheldrick, Crystal structure refinement with SHELXL, Acta Cryst. C 71 (2015) 3–8. https://doi.org/10.1107/S2053229614024218.

[83] O. V. Dolomanov, L. J. Bourhis, R. J. Gildea, J. A. K. Howard, H. Puschmann, OLEX2: a complete structure solution, refinement and analysis program, J. Appl. Cryst. 42 (2009) 339–341. https://doi.org/10.1107/S0021889808042726.

[84] C. M. Aravena, A. C. Olea, H. Cerecetto, M. González, J. D. Maya, J. Rodríguez-Becerra, Potent 5-nitrofuran derivatives inhibitors of *Trypanosoma cruzi* growth: Electrochemical, spectroscopic and biological studies, Spectrochim. Acta A Mol. Biomol. Spectrosc. 79 (2011) 312–319. https://doi.org/10.1016/j.saa.2011.02.007.

[85] G. Kendall, A. F. Wilderspin, F. Ashall, M. A. Miles, J. M. Kelly, *Trypanosoma cruzi* glycosomal glyceraldehyde-3-phosphate dehydrogenase does not conform to the 'hotspot' topogenic signal model, EMBO J. 9 (1990) 2751–2758. https://doi.org/10.1002/j.1460-2075.1990.tb07462.x.

[86] M. D. Lewis, A. Fortes Francisco, M. C. Taylor, H. Burrell-Saward, A. P. McLatchie, M. A. Miles, J. M. Kelly, Bioluminescence imaging of chronic *Trypanosoma cruzi* infections reveals tissue-specific parasite dynamics and heart disease in the absence of locally persistent infection, Cell. Microbiol. 16 (2014) 1285–1300. https://doi.org/10.1111/cmi.12297.

[87] H. Hirumi, K. Hirumi, Continuous cultivation of *trypanosoma brucei* blood stream forms in a medium containing a low concentration of serum protein without feeder cell layers, J. Parasitol. 75 (1989) 985–989. https://www.jstor.org/stable/3282883.

[88] S. Alsford, T. Kawahara, L. Glover, D. Horn, Tagging a *T. brucei* RRNA locus improves stable transfection efficiency and circumvents inducible expression position effects, Mol. Biochem. Parasitol. 144 (2005) 142–148. https://doi.org/10.1016/j.molbiopara.2005.08.009.

[89] T test calculator, GraphPad Software Inc. https://www.graphpad.com/quickcalcs/ttest1.cfm, 2020 (Accessed 28 December 2020).

[90] S. R. Gupta, P. Mourya, M. M. Singh, V. P. Singh, Synthesis, structural, electrochemical and corrosion inhibition properties of two new ferrocene Schiff bases derived from hydrazides, J. Organomet. Chem. 767 (2014) 136–143. https://doi.org/10.1016/j.jorganchem.2014.05.038.

[91] J. Gómez, A. H. Klahn, M. Fuentealba, D. Sierra, C. Olea-Azar, M. E. Medina,

Unsymmetrical cyrhetrenyl and ferrocenyl azines derived from 5-nitrofurane: Synthesis, structural characterization and electrochemistry, Inorg. Chem. Commun. 61 (2015) 204–206. https://doi.org/10.1016/j.inoche.2015.10.007.

[92] C. Quintana, A. H. Klahn, V. Artigas, M. Fuentealba, C. Biot, I. Halloum, L. Kremer, R. Arancibia, Cyrhetrenyl and ferrocenyl 1,3,4-thiadiazole derivatives: Synthesis, characterization, crystal structures and *in vitro* antitubercular activity, Inorg. Chem. Commun. 55 (2015) 48–50. https://doi.org/10.1016/j.inoche.2015.03.008.

[93] J. Bernstein, R. E. Davis, L. Shimoni, N.-L. Chang, Patterns in hydrogen bonding: functionality and graph set analysis in crystals, Angew. Chem. Int. Ed. Engl. 34 (1995) 1555–1573. https://doi.org/10.1002/anie.199515551.

[94] S. J Grabowski, Hydrogen Bonding – New Insights, first ed., Springer, Dordrecht, Netherlands, 2006. https://doi.org/10.1007/978-1-4020-4853-1.

[95] J. A. Bautista-Martínez, I. González, M. Aguilar-Martínez, Influence of the acidity level change in aprotic media on the voltammetric behavior of nitrogabacinamamides, Electrochim. Acta. 49 (2004) 3403–3411. https://doi.org/10.1016/j.electacta.2004.03.008.

[96] B. Aguilera-Venegas, C. Olea-Azar, E. Norambuena, V. J. Arán, F. Mendizábal, M. Lapier, J. D. Maya, U. Kemmerling, R. López-Muñoz, ESR, electrochemical, molecular modeling and biological evaluation of 4-substituted and 1,4-disubstituted 7-nitroquinoxalin-2-ones as potential anti-*Trypanosoma cruzi* agents, Spectrochim. Acta A Mol. Biomol. Spectrosc. 78 (2011) 1004–1012. https://doi.org/10.1016/j.saa.2010.12.017.

[97] C. Olea-Azar, H. Cerecetto, A. Gerpe, M. González, V. J. Arán, C. Rigol, L. Opazo, ESR and electrochemical study of 5-nitroindazole derivatives with antiprotozoal activity, Spectrochim. Acta A Mol. Biomol. Spectrosc. 63 (2005) 36–42. https://doi.org/10.1016/j.saa.2005.04.011.

[98] M. Vieites, L. Otero, D. Santos, C. Olea-Azar, E. Norambuena, G. Aguirre, H. Cerecetto, M. González, U. Kemmerling, A. Morello, J. D. Maya, D. Gambino, Platinum-based complexes of bioactive 3-(5-nitrofuryl)acroleine thiosemicarbazones showing anti-*Trypanosoma cruzi* activity, J. Inorg. Biochem. 103 (2009) 411–418. https://doi.org/10.1016/j.jinorgbio.2008.12.004.

[99] R. Docampo, R. P. Mason, C. Mottley, R. P. Muniz, Generation of free radicals induced by nifurtimox in mammalian tissues, J. Biol. Chem. 256 (1981) 10930–10933.

https://doi.org/10.1016/S0021-9258(19)68534-0.

[100] B. K. Kubata, Z. Kabututu, T. Nozaki, C. J. Munday, S. Fukuzumi, K. Ohkubo, M. Lazarus, T. Maruyama, S. K. Martin, M. Duszenko, Y. Urade, A key role for old yellow enzyme in the metabolism of drugs by *Trypanosoma cruzi*, J. Exp. Med. 196 (2002) 1241–1252. https://doi.org/10.1084/jem.20020885.

[101] C. E. Viodé, N. Bettache, N. Cenas, R. L. Krauth-Siegel, G. E. Chauvière, N. Bakalara, J. Périé, Enzymatic reduction studies of nitroheterocycles, Biochem. Pharmacol. 57 (1999) 549–557. https://doi.org/10.1016/S0006-2952(98)00324-4.

[102] J. D. Maya, Y. Repetto, M. Agosín, J. M. Ojeda, R. Tellez, C. Gaule, A. Morello, Effects of nifurtimox and benznidazole upon glutathione and trypanothione content in epimastigote, trypomastigote and amastigote forms of *Trypanosoma cruzi*, Mol. Biochem. Parasitol. 86 (1997) 101–106. https://doi.org/10.1016/S0166-6851(96)02837-X.